

DEPARTMENT OF PHYSICS, UNIVERSITY OF JYVÄSKYLÄ
RESEARCH REPORT No. 1/1998

**THE MIVOC METHOD
FOR THE PRODUCTION OF
METAL ION BEAMS**

**BY
HANNU KOIVISTO**

Academic Dissertation
for the Degree of
Doctor of Philosophy



**Jyväskylä, Finland
January 1998**

URN:ISBN:978-951-39-9497-6
ISBN 978-951-39-9497-6 (PDF)
ISSN 0075-465X

Jyväskylän yliopisto, 2023

ISBN 951-39-0147-5
ISSN 0075-465X

DEPARTMENT OF PHYSICS, UNIVERSITY OF JYVÄSKYLÄ
RESEARCH REPORT No. 1/1998

**THE MIVOC METHOD
FOR THE PRODUCTION OF
METAL ION BEAMS**

**BY
HANNU KOIVISTO**

Academic Dissertation
for the Degree of
Doctor of Philosophy

To be presented, by permission of the
Faculty of Mathematics and Natural Sciences
of the University of Jyväskylä,
for public examination in Auditorium FYS-1 of the
University of Jyväskylä on February 13, 1998,
at 12 o'clock noon



**Jyväskylä, Finland
January 1998**

PREFACE

This work has been carried out during 1993-97 at the Accelerator Laboratory, Department of Physics, University of Jyväskylä. I would like to thank the laboratory for the excellent working conditions.

I am greatly indebted to my supervisor Dr. Juha Ärje for his support and guidance during this work. I wish to express my gratitude to professor Matti Nurmi for valuable discussions related to this thesis. I would also express my gratitude to the Department of Chemistry, University of Jyväskylä, especially to Dr. Erkki Kolehmainen and Mr. Raimo Seppälä, for pleasant and fruitful collaboration. Special appreciations are extended to the technical staff of the Accelerator Laboratory. I am obliged to professor Matti Nurmi and Dr. Peter Jones for revising the language of the manuscript of this thesis.

The financial support from the University of Jyväskylä, Jenny and Antti Wihuri Foundation, Magnus Ehrnrooth Foundation (The Finnish Society of Sciences), Ella and Georg Ehrnrooth Foundation and the municipality of Nurmo are gratefully acknowledged.

Finally I wish to express my most sincere thanks to my wife Kaisa for her patience, support and encouragement throughout my work. I wish also to express my thanks to my son Tomi for the moments we have spent together.

Jyväskylä, 16 October 1997

Hannu Koivisto

Abstract

A fundamentally new MIVOC method (Metal Ions from Volatile Compounds) for the production of metal ion beams at the ECR ion sources has been developed. With the MIVOC technique it has been found possible to operate the JYFL-ECR ion source with compounds of metals, either powders or liquids, that have vapour pressure of the order of $1\text{E-}3$ mbar, or higher at room temperature.

Up to present time, 17 beams have been produced with the MIVOC method (C, Mg, Si, Cl, Ti, V, Cr, Fe, Co, Ni, Ge, Mo, Ru, Sn, I, W and Os). In every day use it has turned out to be both simple and reliable. Due to this property, the MIVOC method has been adopted at several laboratories.

CONTENTS

1. Introduction	1
2. Theory of ion beam production in an ECR ion source	4
2.1. The operating principle	4
2.2. The physical basis of the operation	5
2.2.1. Plasma frequency ω_p	8
2.2.2. High frequency electromagnetic waves in a plasma situated in a magnetic field	9
2.2.2.a. $\vec{k} \parallel B_0$, Electron Cyclotron Resonance (ECR)	9
2.2.2.b. $\vec{k} \perp B_0$, Upper Hybrid Resonance (UHR)	11
2.2.3. Electron energy E_e	14
2.2.4. Confinement of plasma	15
3. Ion beam production with the ECR ion source	18
3.1. Methods to improve ion beam intensity	18
3.1.1. Increasing the electron density n_e	19
3.1.1.a. Negatively biased electrode	19
3.1.1.b. Plasma cathode method	19
3.1.1.c. Wall coating effect	19
3.1.2. Gas mixing effect	21
3.2. Ion beams from solids	23
3.2.1. Wall recycling	23
3.2.2. Gaseous compounds	24
3.2.3. External oven	24
3.2.4. Insertion technique	26
3.2.5. Other methods	26
4. Experimental facility	28
4.1. The residual gas analyzer: VacScan 100 F	28
4.2. The JYFL-ECR ion source	29
4.3. The K-130 Cyclotron	32
4.3.1. Maximum energy	32
4.3.2. Resolution of analysing magnets and K130 cyclotron	32

5. Optimizing the JYFL-ECRIS for the production of metal ion beams	34
5.1. Basic studies with gases with the JYFL-ECRIS	34
5.1.1. Methods to improve ion beam intensity with the JYFL-ECRIS	34
5.1.1.a. Gas mixing	34
5.1.1.b. The plasma cathode method with gas mixing	35
5.1.1.c. The plasma cathode and the gas mixing method with the aluminium foil liner	36
5.1.2. The gas consumption rate and the gas mixing ratio	37
5.1.3. Gas consumption rate as a function of charge state	40
5.1.4. Studies of ionization efficiencies	41
5.2. The gas feeding system used with the JYFL-ECRIS	43
5.2.1. Introduction	43
5.2.2. Description of the new gas feeding system and its operation	44
5.2.3. Development of the gas feeding system	45
5.2.3.a. Theoretical studies	45
5.2.3.b. Experimental studies	47
6. The MIVOC method	51
6.1. The physical basis of the MIVOC method	51
6.1.1. Minimum vapour pressure required	52
6.1.2. Saturated vapour pressure	53
6.2. Optimization of the metal ion beam production with the MIVOC method	54
6.2.1. A brief history and technical arrangement	54
6.2.2. MIVOC measurements with the residual gas analyzer	56
6.2.2.a. Optimizing the MIVOC chamber	56
6.2.2.b. Determining the minimum sample size and the time to reach vapour saturation	57
6.2.2.c. Average material consumption rate.....	59
6.2.3. Carbon contamination	62
6.2.4. Summary of the development work	63
7. Metal ion beams produced with the MIVOC method	65
7.1. The Mg ion beam	65
7.2. The Si ion beam	67
7.3. The Fe and Ni ion beams	68
7.4. MIVOC beams of Ti, Cr, Co, Cu and Ge	69

7.5. Ion beams from rare isotopes	71
7.6. Cocktail beams	72
7.7. MIVOC compounds used with the JYFL-ECRIS	73
8. Summary and discussion	75
References	78
Appendix (commonly used symbols)	83

1. Introduction

In September 1986 it became possible to replace the old MC-20 cyclotron of the department of Physics, University of Jyväskylä with a new $K=130$ cyclotron. An internal PIG (Penning Ion Gauge) ion source used with the MC-20 had to be replaced by a more versatile ion source.

The energy of the projectile accelerated by the cyclotron is given by the formula

$$E = K \cdot \left(\frac{q}{A}\right)^2 \quad (\text{in MeV/u}), \quad (1.1)$$

where q is the charge and A is the mass number of the accelerated ion. K is a value related to the dimensions and magnetic field of the cyclotron. As equation (1.1) shows, the energy of the projectile depends very strongly on the charge state q of the ion. Thus increasing the charge state by a factor of 2, one can increase the energy by a factor of 4. The cost of such a change is an order of magnitude less than the cost of upgrading the K value by a factor of 4. In the case of K values greater than 300 such an improvement would be beyond the financial resources available for science in Finland.

The performance of a conventional arc ion source is insufficient for the above requirements concerning the charge state. At the present time most of the heavy ion accelerators use an ECR (Electron Cyclotron Resonance) ion source. This kind of ion source can deliver very intensive and highly charged ion beams with high efficiency. In addition the ECR ion source can operate for weeks without interruptions. The use of an ECR ion source with heavy ion accelerators has significantly enhanced their performance in energy, intensity, reliability and variety of ions.

The co-operation to construct the Jyväskylä ECR ion source was started between three Universities: Jyväskylä, Michigan State and Uppsala. The new ion source would be a 6.4 GHz ECR ion source based on the model at the Michigan State University. In 1990 the construction of the JYFL-ECR ion source was started and the first ion beam was extracted in June 1991. The behaviour of the ion source was studied mostly with helium and argon. However, for future applications, different possibilities for producing metal ion beams were also studied.

The ECR ion source can be used to produce ion beams from solids. This greatly extends the repertoire of possible projectile-target combinations, i.e. nuclear reactions. Three main methods have been used for the production of metal ion beams. These methods are: 1) the external oven where the metal is heated upto 2000°C; 2) the plasma heating method (or insert technique) where a rod of a solid compound such as NiO is inserted into the plasma and 3) gaseous compounds. A characteristic for the oven and the plasma heating methods is a more or less violent vaporization of the solid materials at or near high vacuum conditions. Using gaseous compounds the metal ion beams can be produced easily since the ECR ion source can be used in the same way as with normal gases. However, this method has one problem: the lack of convenient gaseous compounds containing the desired element.

In this work a new method to produce metal ion beams has been developed. The MIVOC method (Metal Ions from Volatile Compounds) used with an ECR ion source makes it possible to produce highly charged metal ion beams at room temperature without heating. This method is based on the fact that the ECR ion source needs a very small quantity of material to be ionized. Due to this fact liquid and solid compounds with vapour pressure higher than $\approx 10^{-3}$ mbar at room temperature can be used for the production of metal ion beams.

The second chapter of this work considers the working principle of ECR ion sources and some phenomena related to the production of highly charged ions. The third chapter describes methods to improve the intensity of highly charged ion beams in general and methods related to the production of metal ion beams. The fourth chapter deals with the facility used in this work. In the fifth chapter the JYFL-ECRIS source is optimized for the production of metal ion beams. The sixth and seventh chapters are dedicated to the MIVOC method - its basis, phenomena related to the use of the method, and details about some ion beams produced using this novel technique.

This thesis is partly based on the following published papers:

- [1] J. Ärje, H. Koivisto and M. Nurmiä, Operation of the JYFL-ECR ion source, Proceedings of the 11th International Workshop on Electron Cyclotron Resonance Ion Sources, Groningen, May 1993, p. 27.
- [2] H. Koivisto, J. Ärje and M. Nurmiä, Metal ion beams from an ECR ion source using volatile compounds, Nucl. Instr. and Meth. in Phys. Res. B94, 1994, p.291.
[https://doi.org/10.1016/0168-583X\(94\)95368-6](https://doi.org/10.1016/0168-583X(94)95368-6)
- [3] J. Ärje, H. Koivisto and M. Nurmiä, Status report of the JYFL-ECR ion source, Proceedings of the 12th International Workshop on ECR Ion Sources, RIKEN, April 1995, p.136.
- [4] H. Koivisto, E. Kolehmainen, R. Seppälä, J. Ärje and M. Nurmiä, Production of a magnesium ion beam using the MIVOC method, Nucl. Instr. and Meth. in Phys. Res., B117, 1996, p.186.

[https://doi.org/10.1016/0168-583X\(96\)00238-8](https://doi.org/10.1016/0168-583X(96)00238-8)
- [5] H. Koivisto, M. Hendolin and J. Ärje, New gas feeding system at the JYFL Electron Cyclotron Resonance ion source, Rev. Sci. Instrum. 68 (7), July 1997, p. 2707.

<https://doi.org/10.1063/1.1148183>
- [6] H. Koivisto, R. Harkewicz, J. Ärje and M. Nurmiä, Metal ion beams at the JYFL-ECRIS, Proc. of the 13th Int. Workshop on ECR Ion Sources, Texas, February, 1997, submitted.
- [7] H. Koivisto, J. Ärje and M. Nurmiä, The MIVOC method for the production of metal ion beams, Accepted for publication, Review of Scientific Instruments.
<https://doi.org/10.1063/1.1148539>

2. Theory of ion beam production in an ECR ion source

In the 1980's, the generally used conventional arc sources were increasingly found inadequate for accelerators requiring intensive beams of highly charged ions. At that time two different ion sources, EBIS (Electron Beam Ion Source) and ECRIS (Electron Cyclotron Resonance Ion Source) were being developed. Of these two, the ECRIS has become the favoured ion source to produce heavy ion beams for cyclotrons. In an ECR ion source the bombarding electrons are produced without cathodes which means that there are no wearing parts. The ECR sources have turned out to be very reliable and easy to operate, with a very high availability factor. In addition, the ECR ion source can be used for the production of ion beams of all stable elements.

The roots of the ECRIS history lie in the plasma fusion research of the 1960's. In 1965 Ard et al. [Ard65] pointed out that hot electrons are formed and confined in a simple magnetic mirror container through the coupling of microwaves to the cyclotron resonance of the electrons in the container's magnetic field (device known as an ELMO [Pos70]). The first ion sources using the electron cyclotron resonance heating in order to produce multiply charged ions were reported in 1972 by Geller et al. [Bli72] and by Wiesemann et al. [Ber72]. However, these ion sources had a charge state distribution that was peaked at charge state $q = 2$. Since then, an intense development of the performance of the ECR ion sources has taken place. One of the biggest improvement was made in 1974 when Geller constructed his SUPERMAFIOS which is considered to be the basis of present source design. This source had a hexapole magnetic field which make possible to create so called minimum-B field configuration. The main drawback of this source was the power consumption of 3 MW by the main stage. In order to overcome this problem the next generation ECR ion source was built using permanent hexapole magnets. The summary concerning the historic of the ECRIS can be found for example from [Ari81, Jon89, Gel90, Gel96].

2.1. The operating principle

The ECR ion source can be considered to be a composition of three entities: a magnetic field, a microwave field and low-pressure ionized gas (fig. 2.1). The vacuum chamber is situated inside the magnetic field created by solenoids and hexapole magnets. In the case of the 6.4 GHz JYFL-ECRIS, for example the field strength of this so-called minimum B-structure is between 0.18 T and 0.28 T. It follows from the geometry of the structure that there will exist a closed, egg-shaped surface within the vacuum chamber on which the magnetic field strength is 0.229 T.

A small amount of free electrons is always present in the vacuum inside the ECR ion source. In a magnetic field of 0.229 T the gyrofrequency of electrons is 6.4 GHz. If a matched frequency of microwaves at 6.4 GHz are fed into the vacuum chamber, the electrons on the magnetic surface of 0.229 T are in resonance with the microwaves. Therefore, the electrons in the resonance zone will stochastically gain energy from the electric field \vec{E} of the microwave radiation. The gas of interest is fed into the ion source and ionized by the energetic electrons. The amount of free electrons increases instantly and a plasma confined by the external magnetic fields is created.

The JYFL-ECR ion source is a two-stage ion source. Neutral gas is fed into the first stage where ions of charge state one or two are produced. From there the ions will diffuse into the second stage where highly charged ions will be produced via step-by-step collisions with energetic electrons.

The high vacuum is required to minimize charge exchange reactions between the ions and neutral atoms. The highly charged ions will drift to the extraction end of the ion source due to the diffusion and magnetic configuration. There the ion beam will be extracted by a high voltage into the injection line and transported to the cyclotron.

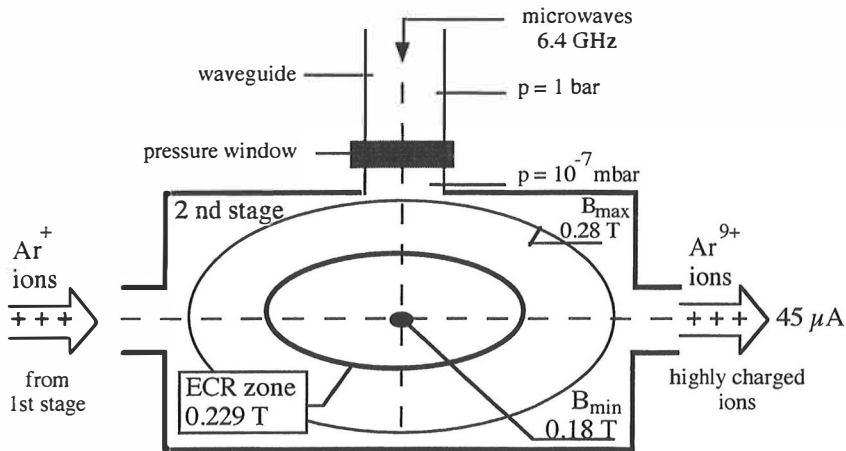


Figure 2.1: A schematic drawing of the ECR ion source operation principle.

2.2. The physical basis of the operation

The behavior of the ECR ion source and the physical phenomena involved are not yet completely understood. Different theories are based on various techniques of simplification such as linearization, cold plasma theory, and single particle theory. A review of the approaches generally accepted by the ECR ion source community is presented below.

In the ECR ion source the bombarding electrons are delivered from the plasma, i.e. not from a cathode. They are accelerated by the electric field component of the microwave perpendicular to the magnetic field due to the electron cyclotron resonance or by upper-hybrid resonance depending on the direction of the propagation of the electric field.

Atoms present in the plasma undergo step-by-step collisions with the electrons. The build up of their charge state is related to the parameter

$$q \propto (n_e \tau_i) E_e \quad (2.1)$$

where n_e is the electron density, τ_i is the confinement time of the ion in the plasma, and E_e is the energy of electron. The rate of the change of the ion density in the ECR plasma at the charge state q is given by

$$\begin{aligned} \frac{dn_q}{dt} = & n_e \langle \sigma_{q-1,q} v_e \rangle n_{q-1} + n_0 \langle \sigma_{q+1,q} v_i \rangle n_{q+1} - n_0 \langle \sigma_{q,q-1} v_i \rangle n_q \\ & - n_e \langle \sigma_{q,q+1} v_e \rangle n_q - \frac{n_q}{\tau} \end{aligned} \quad (2.2)$$

where the first and the second bracket terms are production rates of n_q ions from the charge state $q-1$ to the charge state q by the electron bombardment and from the charge state $q+1$ to the charge state q by the charge exchange reaction. The third and the fourth bracket terms correspond to losses caused by the charge exchange reaction from the charge state q to the charge state $q-1$ and by the ionization from the charge state q to the charge state $q+1$. The last term consists of losses of ions at the charge state q due to the ion diffusion to the wall. $\sigma_{q-1,q}$ is the ionization cross section from the charge state $q-1$ to charge state q and $v_{e,i}$ are the velocities of the electrons and ions, respectively.

The ionization cross-section depends very strongly on the energy of the bombarding electron E_e and on the charge state of the target atom. The cross-sections can be calculated using the Lotz formula [Lotz68]. It has the form

$$\sigma_{q-1,q} = \sum a_i q_i \frac{\ln(E/P_i)}{EP_i} \left\{ 1 - b_i \exp[-c_i(E/P_i - 1)] \right\} \quad (2.3)$$

where $\sigma_{q-1,q}$ is the total ionization cross-section, E the electron impact energy, P_i the binding energy of electrons in the i th subshell, q_i the number of the electrons in the i th subshell and a_i , b_i and c_i are constants given in Lotz's paper.

Figure 2.2 shows examples of the cross-sections of the reactions $Ar \rightarrow Ar^+$ and $Ar^{8+} \rightarrow Ar^{9+}$ as a function of the electron energy. Note that the ionization cross-section decreases three orders of magnitude between the two reactions.

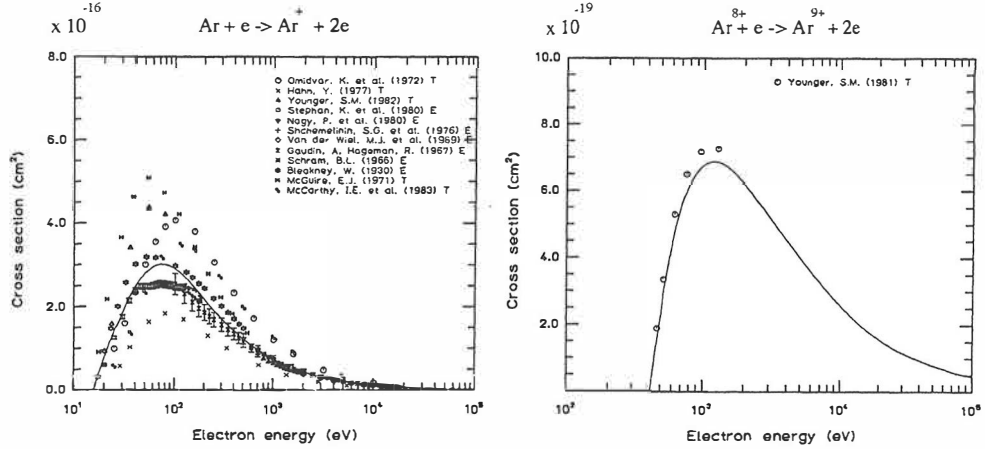


Figure 2.2: The ionization cross-sections for two different charge states of argon [Taw87].

At the ion energies involved with the ECR ion sources the charge exchange cross-section is independent [Mül77,79] or only slightly dependent [Hav89] on the energy of the ions. In this work equation (2.4) [Knu81] has been used to estimate the charge exchange cross-section between highly charged ions and neutrals:

$$\sigma_{q,q-1} = \pi a_0^2 q z^{1/3} (I_0 / I)^{3/2} \quad (2.4)$$

where a_0 is the Bohr radius, I_0 is the Bohr Energy (13.6 eV), I and z are the ionization potential and atomic number of the target atom, respectively. Equation (2.4) shows that the charge exchange cross-section between a charged and a neutral particle of the same species depends only on the charge state of the ion. With the aid of the above equation the charge exchange cross-section between a nitrogen molecule and a Ar^{9+} ion was calculated to be $1.5 \cdot 10^{-15} cm^2$. This shows that the charge exchange cross-section is considerably larger than the ionization cross-section (Fig.2.2) of highly charged ions.

In this chapter some basic phenomena related to the ion beam production using the ECR ion source, i.e. the plasma frequency ω_p , the plasma-wave-interaction, the energy of electrons E_e and the plasma confinement time τ_i will be subsequently described.

2.2.1. Plasma frequency ω_p

Plasma oscillation plays a very important role in the behavior of the ECR ion sources. Externally created electromagnetic waves of frequency higher than a critical frequency can propagate into the plasma, while waves at lower frequencies are reflected from the plasma boundary. This critical frequency is known as the cutoff frequency.

Consider a plasma containing equal numbers of positive ions and electrons with a uniform charge distribution. If the electrons in the plasma are displaced from their initial position, an electric field will be formed in the plasma in order to restore its quasi neutrality. This field will accelerate the electrons toward their original position and cause them to oscillate around it with a characteristic frequency known as the plasma frequency. This oscillation is so fast that the massive ions remain in a fixed position [Eng83].

Based on Poisson's equation, the angular frequency of the plasma oscillation ω_p is obtained as

$$\omega_p = \left(\frac{e^2}{m_e \epsilon_0} n_e \right)^{1/2} \quad (2.5)$$

where e is the elementary charge, n_e is the electron density, m_e is the electron mass and ϵ_0 the permittivity constant. Equation (2.5) shows that the plasma frequency depend only on the electron density n_e . Therefore, the equation (2.5) can be expressed in a more convenient way as

$$f_p \cong 9000 \sqrt{n_e} \text{ Hz}, \quad [n_e] = \text{cm}^{-3} \quad (2.6)$$

With the aid of equation (2.6) the cutoff plasma density n_c for a microwave frequency of 6.4 GHz is determined to be

$$n_c = 5 \cdot 10^{11} / \text{cm}^3 \quad (2.7)$$

2.2.2. High frequency electromagnetic waves in a plasma situated in a magnetic field

The energy of the plasma electrons comes from the incident electromagnetic wave energy. In the case of the ECR ion source it is reasonable to divide electromagnetic waves into two classes: waves propagating parallel to the external magnetic field \vec{B}_0 , $\vec{k} \parallel \vec{B}_0$, and waves propagating perpendicular to the external magnetic field \vec{B}_0 , $\vec{k} \perp \vec{B}_0$. Here $k = 2\pi/\lambda$ is the wave number which describes the direction of the propagation. The reflection and the resonance of the electromagnetic wave occurs when $\vec{k} \rightarrow 0$ or $\vec{k} \rightarrow \infty$, respectively.

The propagation of the electromagnetic wave in the plasma can be described with the aid of equation (2.8)

$$m \frac{d\vec{v}}{dt} = -e(\vec{E} + \vec{v} \times \vec{B}_0) \quad (2.8)$$

and with the aid of the wave equation defined from the Maxwell equations

$$k^2 \vec{E} - \vec{k}(\vec{k} \cdot \vec{E}) = (\omega^2 / c^2)[\vec{E} + i\vec{j}/(\epsilon_0 \omega)] \quad (2.9)$$

where \vec{E} is the electric field, \vec{B}_0 is the external magnetic field, \vec{v} is the velocity of the charged particle, c is the velocity of light, ω is the microwave frequency, $\vec{j} = -n_{e0}e\vec{v}$, and n_{e0} the zero-order electron density. The electromagnetic wave is assumed to propagate perfectly perpendicular or parallel to the external magnetic field B_0 , which is assumed to be parallel to the z-axis.

2.2.2.a. $\vec{k} \parallel \vec{B}_0$, Electron Cyclotron Resonance (ECR)

In this case we are considering the propagation of the electromagnetic wave propagating parallel to the external magnetic field, i.e. $\vec{k} \parallel \vec{B}_0$. In addition, \vec{E} is allowed to have components E_x and E_y . From equations (2.8) and (2.9)

$$\tilde{n}^2 = \frac{c^2 k^2}{\omega^2} = 1 + \frac{\omega_p^2 (\omega \mp \omega_c)}{\omega(\omega_c^2 - \omega^2)} = 1 - \frac{\omega_p^2}{\omega(\omega \pm \omega_c)} \quad (2.10)$$

where \tilde{n} is the index of refraction, ω_p is the plasma frequency, $\omega_c = |e|B/m_e$ is the gyrofrequency of electrons and ω is the frequency of microwaves. Equation (2.10) is the dispersion relation of the circularly polarized waves. Upper signs, L-wave, correspond to the wave rotating according to a left-hand rule, and lower signs, R-wave, correspond to the right-hand rule. Figure 2.3 shows the R-wave in the magnetized plasma.

Equation (2.10) shows that something interesting will happen when $\omega = \omega_c$. For the R-wave k becomes infinity; the wave has a resonance with the cyclotron motion of the electrons. The wave loses its energy, continuously accelerating electrons, consequently the wave cannot propagate anymore. This is exactly the way ionization is caused in the ECR ion source: the accelerated electrons bombard gas atoms and liberate their orbital electrons.

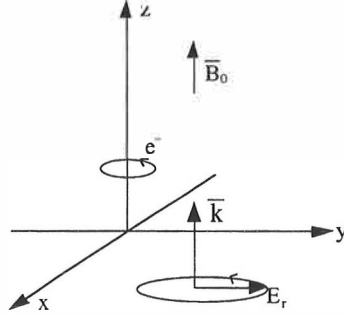


Figure 2.3: R-wave in the magnetized plasma.

Figure 2.4. shows the dispersion diagram of the circularly polarized wave according to equation (2.10). The magnetic field B_0 of the strength of 0.229 T was used in the calculation. At this strength of magnetic field the gyrofrequency of electrons equals the 6.4 GHz microwave frequency used at the JYFL-ECRIS. Electrons have a resonance when $1/\tilde{n}^2 \rightarrow 0$, i.e. when $k \rightarrow \infty$. Figure 2.4 shows that only the right-hand polarized wave has a resonance at $\omega_c = 6.4\text{GHz}$. The wave does not propagate in the region where $1/\tilde{n}^2 < 0$.

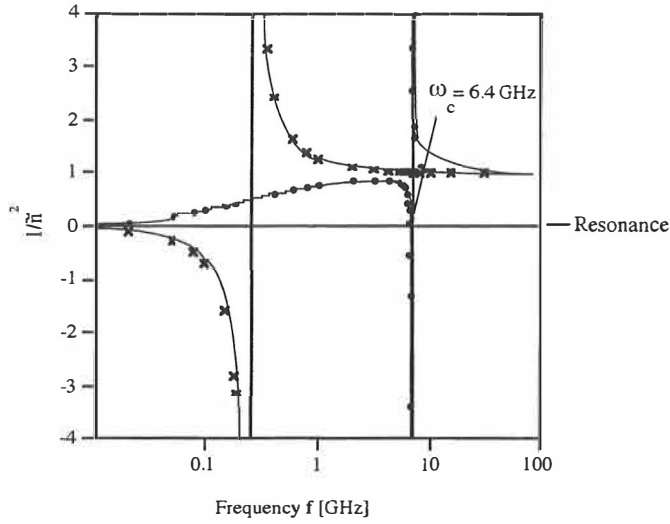


Figure 2.4: The dispersion diagram of the L- and R-waves. Crosses correspond to the L-wave and black dots correspond to the R-wave. Resonance occurs where $1/\bar{n}^2 = 0$.

2.2.2.b. $\vec{k} \perp \vec{B}_0$, Upper Hybrid Resonance (UHR)

In this section, the case where the electromagnetic wave propagates perpendicularly to the external magnetic field B_0 will be discussed. These electromagnetic waves can be divided into two classes: “ordinary” and “extraordinary” waves. Only the extraordinary wave has a resonance with the gyromotion of the electrons. The direction of the wave’s magnetic field is chosen to be parallel to the z axis and the direction of the propagation of the electromagnetic wave is chosen to be parallel to the x axis, i.e. perpendicular to the magnetic field. Figure 2.5 shows the extraordinary wave propagating in the magnetized plasma.

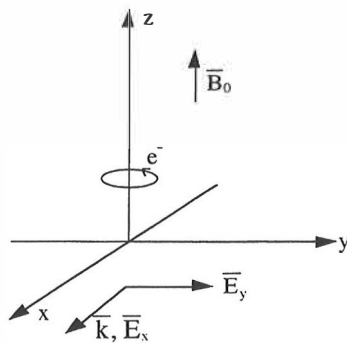


Figure 2.5: The extraordinary wave in the magnetized plasma.

Inside the plasma the extraordinary wave has both a transverse and a longitudinal component, i.e. $\vec{E} \parallel \vec{k}$ and $\vec{E} \perp \vec{k}$. In addition the external magnetic field is perpendicular to the electrical component of the wave. Using equations (2.8) and (2.9), Eq. (2.11) is obtained:

$$\tilde{n}^2 = \frac{c^2 k^2}{\omega^2} = \frac{c^2}{v_p^2} = 1 - \frac{\omega_p^2(\omega^2 - \omega_p^2)}{\omega^2(\omega^2 - \omega_h^2)} \quad (2.11)$$

where the “upper-hybrid” frequency is defined as

$$\omega_h^2 \equiv \omega_p^2 + \omega_c^2 \quad (2.12)$$

The upper hybrid resonance occurs when the condition $\omega = \omega_h$ is fulfilled. It has been assumed that UHR dominates ECR heating when $\omega_p^2 / \omega_{RF}^2 \geq 0.1$ [Gel93]. This means that the electron density of the plasma has to exceed the value of $0.1n_c$. At this point the strength of the magnetic field has to be 0.217 T in order to have the UHR in the JYFL-ECRIS. If the electron plasma density increases the UHR region moves towards the decreasing magnetic field. Since the minimum magnetic field inside the JYFL-ECRIS is 0.18 T the maximum electron plasma density for UHR is $0.36n_c$. As a consequence, the following conditions for the magnetic field and the electron densities are obtained in order to have upper hybrid resonance at the JYFL-ECRIS:

$$\begin{aligned} 0.1n_c &= 5 \cdot 10^{10} / cm^3 \leftrightarrow 0.217T \\ 0.36n_c &= 1.8 \cdot 10^{11} / cm^3 \leftrightarrow 0.18T \end{aligned} \quad (2.13)$$

The electron densities above more likely appear in the first stage plasma chamber.

Figure 2.6 shows the dispersion diagram of the extraordinary wave obtained using equation (2.11) when the strength of the magnetic field B is chosen to be 0.215 T. In order to fulfill the requirement $\omega_h^2 \equiv \omega_p^2 + \omega_c^2 = (6.4GHz)^2$, the electron density of the plasma has to be $n_e = 6 \cdot 10^{10} \text{ electrons} / cm^3$. As a consequence, the extraordinary wave has a resonance at ω_h .

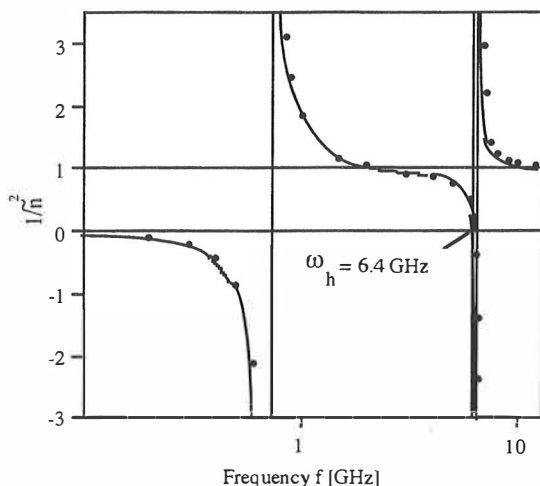


Figure 2.6: The dispersion diagram of the extraordinary wave obtained using equation (2.11). Resonance occurs where $1/\tilde{n}^2 = 0$.

As was shown above, only the extraordinary wave and R-wave have a resonance with electrons. In the case of the right-hand polarized wave the heating of electrons takes place at the ECR resonance. The extraordinary wave penetrates through the ECR surface without seeing it. In this case the heating takes place at the UHR resonance [Gol93]. Due to the resonance (ECR or UHR) with microwaves, electrons are accelerated to the high energy necessary to produce highly charged ions.

Up to the present time the ECR resonance was believed to be the more efficient for the production of highly charged ions. The UHR resonance was believed to be efficient when high-current ion beams with a low charge state distribution were produced. A very interesting theory concerning the heating of the ECR plasma electrons has been developed by Golovanivsky [Gol95]. He assumed that the extraordinary wave is converted into electrostatic Bernstein waves [Ber58] near the UHR resonance zone. The Bernstein wave will have a resonance at $B=B_{ECR}/m$, where $m = 1, 2, \dots$. In a conventional ECR ion source the microwave field has a resonance at the ECR, when a hot corona will be produced. If the magnetic field near the axis has a zone where the condition $B=B_{ECR}/2$ is fulfilled, a very hot core plasma will be obtained.

2.2.3. Electron energy E_e

As was shown in figure 2.2, the ionization cross-section depends very strongly on the energy of the electron and on the charge state of the ion. Very energetic electrons are needed to achieve highly charged ions. The power input of microwaves is the key parameter related to the electron energy. Figure 2.7 shows the energy of the electrons as a function of the microwave power P_μ .

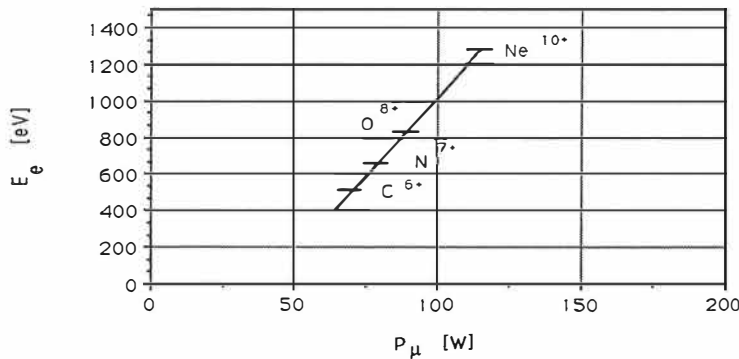


Figure 2.7: The energy of the electrons as a function of the microwave power P_μ [Gel83].

The energy of the electrons increases or decreases when they pass the resonance zone depending on their phase with the microwaves. As an example, figure 2.8 shows how the energy of electrons change when they pass the resonance zone several times. This has been simulated with an aid of the TrapCAD code [Bir95]. The four different curves correspond to four different starting phases of the electrons. The energy of all electrons will increase in proportion to the wave energy density $|\bar{E}|^2$ [Gel93].

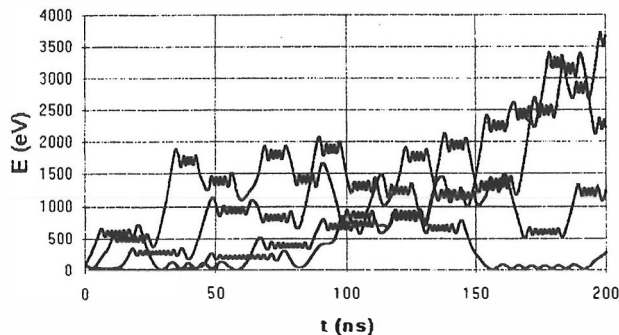


Figure 2.8: An example of the energy of the electron as a function of the ECR heating time for four electrons with a different initial phase. The energies are simulated using TrapCAD [Bir95].

2.2.4. Confinement of plasma

The charge state of the ions increases with increasing ion confinement time τ_i . The confinement time can be increased by decreasing the energy of the ions (by gas mixing) or increasing the mirror ratio of the magnetic bottle, $R = B_{\max}/B_{\min}$. The velocity component parallel to the magnetic field, v_{\parallel} , of a particle will vary when it moves into regions of different magnetic field strengths of the magnetic field according to

$$mv_{\parallel}^2 / 2 = E_k - \mu B, \quad (2.14)$$

where E_k is the kinetic energy of the charged particle and

$$\mu \equiv \frac{1}{2}mv_{\perp}^2 / B \quad (2.15)$$

is its magnetic moment [Che74]. Since μ is constant, the parallel velocity v_{\parallel} decreases with increasing magnetic field B . If B is high enough, the parallel velocity becomes zero and the particle is reflected back toward the decreasing magnetic field, i.e. the particle is trapped inside the magnetic bottle. If we denote the minimum magnetic field by B_{\min} and maximum magnetic field by B_{\max} , then the trapping takes place when the condition $\mu > E_k/B_{\max}$ is fulfilled. Figure 2.9 shows a plasma trapped between the magnetic mirrors created by a pair of coils.

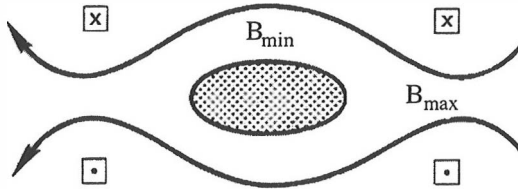


Figure 2.9: A plasma trapped between magnetic mirrors [Che74].

The loss cone defines the fraction of the particles which are able to escape from the magnetic bottle at a given magnetic field. The initial velocity components of the particle are denoted by $v_{\perp} = v_{\perp 0}$ and $v_{\parallel} = v_{\parallel 0}$. The corresponding values at the turning point are denoted by dots. The invariance of the μ yields

$$\frac{1}{2}mv_{\perp 0}^2 / B_{\min} = \frac{1}{2}mv_{\perp}^2 / B' \quad (2.16)$$

where B' is the magnetic field at the turning point. Using a conservation of energy and equation (2.16) Eq. (2.17) is obtained

$$\frac{B_{\min}}{B'} = \frac{v_{\perp 0}^2}{v_{\perp}^2} = \frac{v_{\perp 0}^2}{v_0^2} \equiv \sin^2 \theta \quad (2.17)$$

Replacing B' by B_{\max} in equation 2.17 the minimum θ_m of a confined particle can be found. Figure 2.10 shows the loss cone in the velocity space. The magnetic loss cone is independent of the charge and mass of the particles [Gold95]. In the ECRIS the axial confinement is obtained using solenoids and the radial confinement using multipole magnets.

Due to collisions with each other, the particles change their direction of velocity and can escape from the plasma. When the temperatures of the ions and electrons are equal, i.e. $T_i \approx T_e$, the higher collision frequency of the electrons leads to a higher loss rate of electrons from the plasma. As a consequence a positive electric charge will build up in the plasma which regulates the loss of low energy electrons.

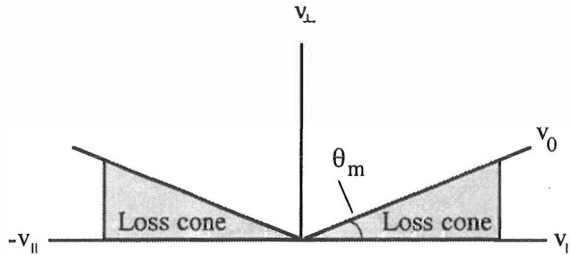


Figure 2.10: Velocity space loss cone in a magnetic mirror [Che74].

In the ECR ion source the heated electrons have orders of magnitude higher temperature than the ions, i.e. $T_e \gg T_i$. As a consequence the electrons have a much smaller probability to collide with the other species. The relatively high rate of ion loss creates the negative plasma voltage which regulates the loss of ions. This electrostatic potential well confines the positively charged ions inside the ECR plasma [Gol90, Shi92b, 95].

The height of the potential well can be increased by increasing the temperature of the electrons [Nii95] or the mirror ratio. In the case of the JYFL-ECRIS the mirror ratio can be varied between 1.2 - 2.2. Considerable improvement of the ion intensities has been achieved with many ECR ion sources using a strong magnetic field resulting in a high magnetic mirror ratio R . An example of this is the so-called $2 \omega_{ce}$ source constructed in Grenoble [Jac90]. This means that the maximum magnetic field within the plasma chamber is at least twice as large as the resonance field [Hit93]. The mirror ratio is as high as 3.5. For example, with this Caprice source the intensity of Ar^{13+} was raised from $0.5 \mu\text{A}$ to $12 \mu\text{A}$ [Hit95]. Similar results were achieved at MSU using so called high-B mode [Ant94]. Nowadays, all new ECR ion sources are constructed with a high magnetic mirror ratio.

As figure 2.2 shows, the ionization cross-section decreases dramatically when higher charge state is required. In order to maximize the yield of the highly charged ions, the electron density or the lifetime of the ions has to be increased. Different methods to accomplish this goal will be described in the following chapters.

3. Ion beam production with the ECR ion source

A small amount of the appropriate gas is fed into the ECR ion source to be ionized by hot electrons. The typical gas feed rate is of the order of $1 \text{ cm}^3/\text{h}$ at NTP conditions (NTP = normal temperature and pressure). Figure 3.1 shows the influence of the conditions in the ECR ion source on the mass spectrum of the extracted argon beam. The measured beam current is shown here as a function of the current in the analysing magnet. The right hand picture corresponds to the situation when the ECR ion source was carefully tuned and nitrogen was mixed into the plasma to enhance the current of the highly charged argon ions. As a result, the intensity of Ar^{9+} ion beam was increased by a factor of 3.

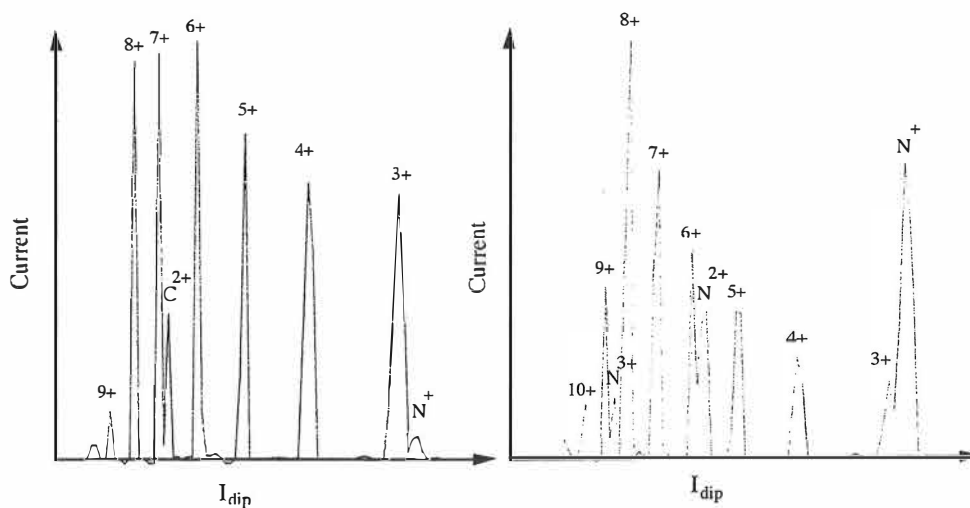


Figure 3.1: Argon mass spectra extracted from the ECR ion source.

The ECR ion source can be used for the production of metal ion beams, too. The material of interest has to be in a gaseous state before ionization, and different methods are used to vaporize the materials that are solids at room temperature. The most commonly used methods for the production of metal ion beams will be discussed in section 3.2.

3.1. Methods to improve ion beam intensity

The most important feature of the ECR ion source is its ability to produce highly charged ions. Many methods have been studied to improve this property. The production

probability of ions is assumed to be proportional to the product $n_e \cdot \tau_i$. As a consequence of the above mentioned rule, the production of highly charged ions can be improved by increasing the density of electrons in the plasma or by lengthening the confinement time of the ions. The most commonly used techniques to enhance the ion beam intensity are discussed below.

3.1.1. Increasing the electron density n_e

3.1.1.a. Negatively biased electrode

A negatively biased disk or floating disk has been installed in a few ECR ion sources [Mel90, Gam92]. When a negative voltage with respect to the plasma is used, the intensity of the extracted output current of highly charged ions is increased by a factor two to three [Fri93] or even more depending on the produced charge state of the ion. The electron density of the plasma increases due to the secondary electron emission produced by the plasma particles colliding with the electrode. A similar improvement can be achieved using an electron gun [Lyn90].

3.1.1.b. Plasma cathode method

Nakagawa [Nak92,93] noticed that the intensity of highly charged ions increased when the 1st stage plasma chamber is electrically isolated from the 2nd stage and a potential difference is applied between the stages. The intensity of highly charged ions increases steeply as a function of the bias voltage on the 1st stage. The maximum beam current is normally reached at 200-400 V potential difference. After that an increase in the bias voltage does not increase the intensity of the ion beam. The intensity of highly charged ions, for example Ne^{7+} , is enhanced even by a factor of 10. The main advantage of the plasma cathode method is long lifetime compared to the negatively biased electrode which has to be replaced after two months of operation. This method has been used with the JYFL-ECRIS.

3.1.1.c. Wall coating effect

Lyneis et al. noticed that the O^{7+} and O^{8+} currents were greatly increased after a SiH_4 run when oxygen was used as a mixing gas [Lyn87]. The mixing gas is the component in the gas mixture that maintains the major part of the plasma. As an example the O^{7+} ion beam increased from 6 μA to 12 μA after Si ion beam production. Geller and his group noticed that the intensity of an argon beam was improved after calcium and

tantalum runs [Gel87]. They gave arguments that coating the wall with materials of low work function increases the supply of electrons. Nakagawa observed an enhancement of the intensity of highly charged argon ion beams after the production of Al and Mg ion beams using Al_2O_3 and MgO rods with the insertion technique [Nak90]. As an example, after the aluminium run the intensity of Ar^{14+} increased by a factor of 6 compared to a normal argon run.

The wall coating affects the electron density because of the different secondary electron emission yields of the different materials. The improvement can be accomplished either by using suitable materials inside the plasma chamber or by allowing the materials to be deposited on the walls due to the incomplete confinement of the plasma, for example during a magnesium run. The material of the plasma chamber of the ECR ion source is usually copper, aluminium or stainless steel. Figure 3.2 shows a typical secondary electron emission distribution as a function of primary electron energy.

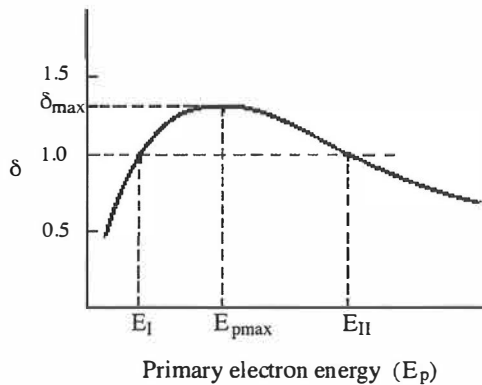


Figure 3.2: The secondary electron emission yield as a function of the energy of primary electron [CRC77].

Table 3.1 shows the secondary electron emission properties of some elements and compounds. δ_{max} is the maximum yield corresponding to a primary electron energy E_{pmax} . E_I and E_{II} are the first and second crossovers as defined in Fig. 3.2. The secondary electron emission yields of Al_2O_3 and MgO are much higher as those of Cu or Cu_2O . This explains why a wall coating of oxidized Al or Mg acts as a supply of additional electrons. The oxidization of the pure Al or Cu surface can be accomplished by running the source with oxygen

<i>Element</i>	δ_{max}	E_{pmax} [eV]	E_I [eV]	E_{II} [eV]
Al	1.0	300	300	300
Cu	1.3	600	200	1500
C (soot)	0.45	500	none	none
Cu ₂ O	1.2	400	-	-
Al ₂ O ₃	2-9	-	-	-
MgO	3-15	400-1500	-	-
SiO ₂ (quartz)	2-4	400	-	-

Table 3.1: Secondary electron properties of elements and compounds [CRC77].

3.1.2. Gas Mixing Effect

The first observations related to the gas-mixing effect were made by A.G.Drentje [Dre85] and H.Beuscher [Beu85]. They noted that the intensity of highly charged ions was greatly improved when a lighter element was mixed into the plasma. Typically, helium, nitrogen or oxygen are used as a mixing gas. Experimental results give, as a rule of thumb, $Z_{mix} \leq Z_{ion}/2$ for good gas-mixing effect [Ant89]. Here Z_{mix} is the Z of the mixing gas and Z_{ion} that of the ion gas. "Ion gas" here means the element for the ion beam to be used when a mixing gas is the gas used to maintain the main plasma. M.Mack et al. reported the best mixing ratio to be 40/60 for the Ar/He and 20/80 for the Ar/N₂ mixture [Mac86]. The Jülich group reported the best mixing ratio to be as low as 3/97 for an Ar/N₂ mixture.

Several explanations have been given for the gas mixing effect:

- 1) Geller has given arguments that the average charge state of heavy ions can be enhanced by the mixing gas [Gel87]. The gas mixing increases the lifetime of the electrons inside the plasma. As the energy of the microwaves is mainly transferred to the electrons, the energy-lifetime is increased and a lower RF-power input can be used. This decreases the level of turbulence in the plasma and the intensity of the extracted ion beam will be increased. The ECR ion source can be operated far below the threshold of the turbulence, thus leading to better confinement of highly charged ions.
- 2) Antaya reported that the energy spread of Ar⁹⁺ is reduced when using oxygen as a mixing gas [Ant89]. As a conclusion, it was emphasized that ion - ion collisions transfer energy from the heavier to the lighter species so that the energy of the heavier ions decrease. This ion cooling effect leads to a better confinement of the heavy ions. This theory has been confirmed using another experimental setup by Drentje [Dre92]. The same results have been achieved theoretically by Shirkov [Shi92a].
- 3) Delaunay has given arguments that the electron density, n_e , depends upon the ionization of the support gas [Del92]. In other words, the mixing gas behaves as an additional source of electrons analogous to an electron gun or a wall coating.

The question of the ion cooling can be approximately studied by assuming a one-dimensional elastic head-on-collision [Koi97b]. The energy of the ion has experimentally shown to be $(6-40)q$ eV, depending on the operation of the ECR ion source [Mey85]. In this calculation the energy of ions were assumed to be $6 \cdot q$ eV before the collision. The velocity of the heavier ion after the collision was calculated with the aid of equation (3.1) obtained using the conservation of energy and momentum

$$V_1 = \frac{(M - m)V_0 + 2mv_0}{m + M} \quad (3.1)$$

where M and V are the mass and velocity of the ion gas element and m and v are corresponding factors of the mixing gas element. The velocities of the elements before and after the collisions are represented by subscripts 0 and 1, respectively. The velocity of the mixing gas ion can be calculated when the velocity of the heavier ion is known.

As an example, the cooling effect of the Fe^{12+} ion is calculated when it collides with different mixing gas ions. Here the charge state of 12 was used since it is the most commonly used charge state of iron ions with the JYFL-ECRIS. The following mixing gas ions were used in the calculations: H^+ , H_2^+ , He^+ , C^{2+} , N^{3+} , O^{4+} , Ne^{5+} , Si^{6+} and Ar^{7+} . These charge states are assumed to be very abundant from their spectra.

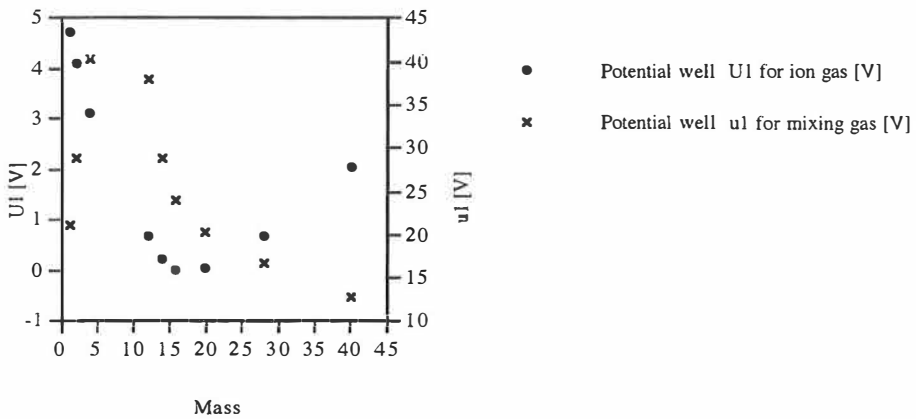


Figure 3.3: The depth of the plasma potential well required to confine Fe^{12+} and different mixing gas ions after a head-on collision as a function of the mass of the mixing gas. Note the different scales.

As previously described in section 2.2.4. a potential difference is built up between the walls and the ECR-plasma. This potential regulates the loss of ions. Since the velocity of the ions is known, the voltage to stop them can be calculated. Figure 3.3 shows the voltage necessary to stop the Fe^{12+} ions, i.e. the voltage to confine them in the plasma,

when it has collided with the above mentioned mixing gas ions. Here U_1 and u_1 correspond to the voltages needed to confine Fe^{12+} ions and mixing gas ions, respectively. The calculation suggested that the best cooling element for Fe^{12+} ions is oxygen or neon. The voltages to confine Fe^{12+} and Ne^{5+} ions after the collision are approximately 0.1 and 20 volts, respectively. This indicates that the confinement of Fe^{12+} ion is much better than that of neon. Proceeding the same way, helium was found to be the best cooling element for the N^{5+} ions and nitrogen and oxygen best for the Ar^{8+} ions. Similar results have experimentally been achieved also by other groups [Dre93]. Figure 3.3 reveals also that hydrogen and helium are not very efficient cooling elements for heavy ions.

3.2. Ion beams from solids

The characteristics of the ECR ion source make it possible to use very heavy projectiles in accelerators. However, only a few heavy elements are in a gaseous state at room temperature. To extend the repertoire of accelerated beams to those from solid elements, a method has to be used to vaporize them before the ionization process. The selection of the appropriate method depends on the properties of the desired element and the design of the ECR ion source. In the following chapters the main methods used for metal ion beam production will be described: 1) wall recycling, 2) external oven, 3) insertion technique 4) gaseous compounds and 5) other methods - in particularly the MIVOC method developed during this work.

A few additional factors make the production of metal ion beams more difficult compared to gases: the control of the material feed rate, contamination of the walls of the plasma chamber and the complexity of the devices needed to introduce the metal. In the production of solid ion beams, the material feed rate, i.e. the vaporization rate of the material, is changed by changing its temperature (in the oven method) or by changing its position (in the insertion method). This results in a long time constant making the tuning of the ion source difficult. A considerable part of the metal vapour produced can escape to the walls of plasma chamber and cause contamination. The need to supply heating power to the oven, as well as the need for mechanical movement of the rod in the insertion method, result in these devices becoming rather complex and expensive.

3.2.1. Wall recycling

The wall recycling method was described by Geller et al. in the early 80's [Bou82]. This method is carried out in two different phases. In the first phase the sample is heated inside the ECR ion source to deposit some of the material onto the walls of the vacuum chamber. This first phase is done without a plasma in the ECR ion source and special

care has to be taken to avoid excessive warming of the permanent magnets. In the actual operation the solid material is reevaporated from the walls by the sputtering process. Reevaporated atoms are confined and ionized by the hot electrons of the plasma. The wall recycling process is always present to some extent when metal ion beams are produced. This is exploited in the wall coating method.

3.2.2. Gaseous compounds

Some solid ion beams can be produced with the aid of the gaseous compounds containing the desired element, such as carbon in CO_2 or silicon in SiH_4 . This method is the simplest way to produce metal ion beams. The ECR ion source can be used in the same way as in the case of normal gases. This method also gives the best long-term stability - even weeks without problems. The gaseous compound is fed into the ECR ion source where the molecules are dissociated and ionized by the energetic electrons. As an example, the following ion beams have been produced by using gaseous compounds: B (BF_3), C (CO_2), F (CHF_3), Si (SiH_4), S (SH_2), Cl (CCl_4) and U (UF_6).

3.2.3. External oven

The oven technique was mainly developed by Clark and Lyneis at Berkeley. The oven is radially mounted to the second stage plasma chamber. The metal vapour flows directly into the plasma where it is ionized by hot electrons. The contamination of the plasma chamber and the consumption rate of material are minimized by feeding the material directly into the second stage. This is important when using rare isotopes.

The normal consumption rate is a few mg/h. For many nuclear physics experiments only a very low intensity is needed. As an example the consumption rate of 0.15 mg/h of ^{48}Ca has been reported [Lyn87]; during the run 0.6 μA of $^{48}\text{Ca}^{11+}$ was extracted from the ECRIS. During production of a high intensity, low charge state iron ion beam, a consumption rate of 30 mg/h was measured by Clark [Cla88].

A so-called low temperature oven is shown in figure 3.4 [Lyn87,Cla88]. The source material is placed in a tantalum crucible that is heated by conduction from the heater section. The normal operation temperature is up to a few hundred degrees C (max. $\approx 700^\circ\text{C}$). The input rate of the material is controlled by changing the temperature of the oven. The time constant for the temperature control is a few minutes and cooling of the oven for recharge can also be accomplished in a few minutes. However, several hours of pumping is needed to reach the required operating pressure.

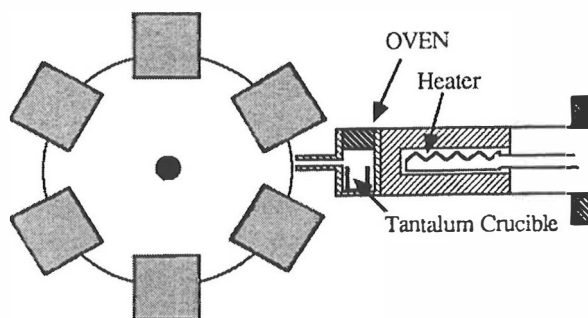


Figure 3.4: Schematic drawing of a low temperature oven (modified from [Cla88]).

A high-temperature oven has been designed for elements with a high melting point [Cla88]. A maximum operating temperature of 2000°C is reached by passing ac current directly through a tantalum crucible. This way a very uniform heating is reached to prevent the condensation of vapour at the crucible's exit aperture. An exit hole of about 3 mm diameter, pointing towards the axial center line of the plasma chamber is used.

The most modern oven technique is the so-called miniature oven [Hit93, Har96]. It has turned out to be very efficient and easy to use. From this oven the vapour can flow directly into the ECR plasma (Fig. 3.5). As a consequence the material consumption rate is very low, even less than 0.1 mg/h. The power consumption of the oven is on the order of 20-30 W.

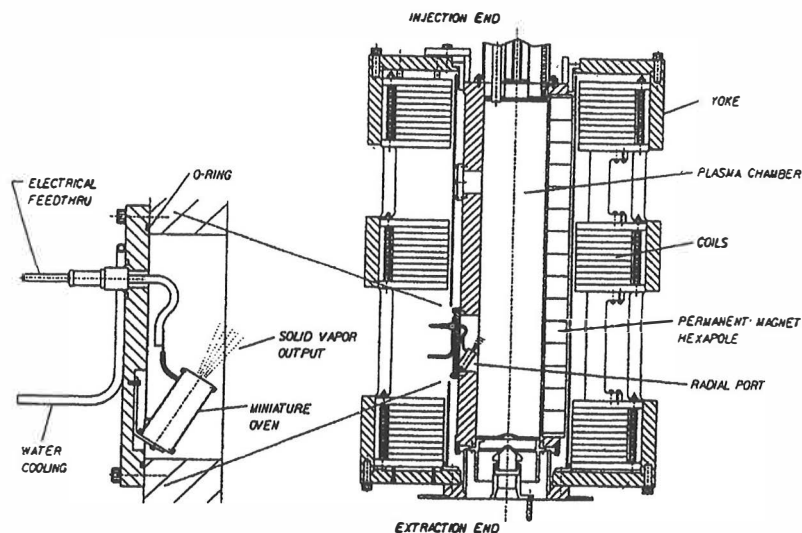


Figure 3.5: The miniature oven in the JYFL-ECR ion source [Har96].

3.2.4. Insertion technique

The insertion technique [Gel92] has mainly been developed by the Grenoble team [Gel86] and later by the RIKEN team [Nak90]. This technique has been practically the only possibility to produce an intensive, highly charged ion beam from the refractory elements. Figure 3.6 shows the principle of this method.

The insertion technique is based on the bombardment of the sample by energetic plasma electrons. The metal or ceramic rod is inserted usually radially into the plasma chamber. The hot electrons collide with the rod transferring their kinetic energy to the material. The vaporization rate of the material can be changed by varying the position of the rod, the flow of mixing gas, and the microwave power. The normal consumption rate of the rod with a diameter of 4 mm is 0.4 mm/hour for all elements, i.e. a few mg/h [Nak90]. A method of inserting thin foils of the metal into the edge of the ECR plasma is also used [Mey90].

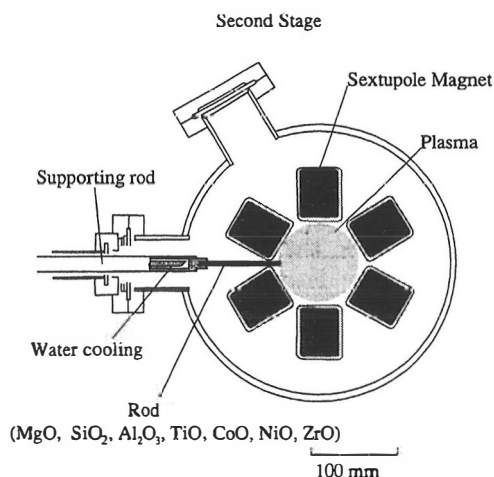


Figure 3.6: Schematic drawing of the insertion technique [Nak95].

3.2.5. Other methods

New and more elaborate methods have been developed to produce a metal ion beam with an ECR ion source. The laser ablation method [Har94] makes it possible to produce metal ion beams efficiently from very small quantities of material while avoiding any interference with the plasma. Depending on the laser power any material can be vaporized. Harkewicz has also noted that plasma sputtering can be used to introduce solid material into the ECR plasma [Har95].

Y. Yamashita et al. have developed the so-called metal liner method where metal ion beams from refractory elements can be produced very efficiently with minimum

disturbance of the plasma [Yam95]. The electron bombardment is very effective for solids whose melting point is over 2500°C. With this method the electrons from an electron gun are accelerated by a high voltage into a crucible containing the metal sample. The evaporated material is then ionized by the hot plasma electrons [Yam95].

The most novel technique to produce ion beams from solid elements is called MIVOC (Metal Ions from Volatile Compounds) [Koi94]. Details of this technique are presented in the following chapters.

4. Experimental facility

Development work on metal ion beams by the MIVOC method has been carried out in two phases: First, properties of interesting compounds were studied by connecting the MIVOC chamber to a residual gas analyzer. This way the partial pressures of the constituents can be measured simply and reliably. In the second phase the same MIVOC chamber containing the metal compound was connected to the second stage of the JYFL-ECR ion source in order to study the production of highly charged metal ion beams. The performance of the JYFL-ECRIS in producing highly charged beams is only moderate. Consequently, only elements lighter than krypton were investigated.

4.1. The residual gas analyzer: VacScan 100 F

At first the properties of the interesting compounds were investigated with the residual gas analyzer. A small vacuum chamber loaded with the volatile compound is connected to the analyzing chamber, where the vapour of the compound is admitted. The composition of the gas inside the chamber is measured using the residual gas analyzer VacScan 100 F.

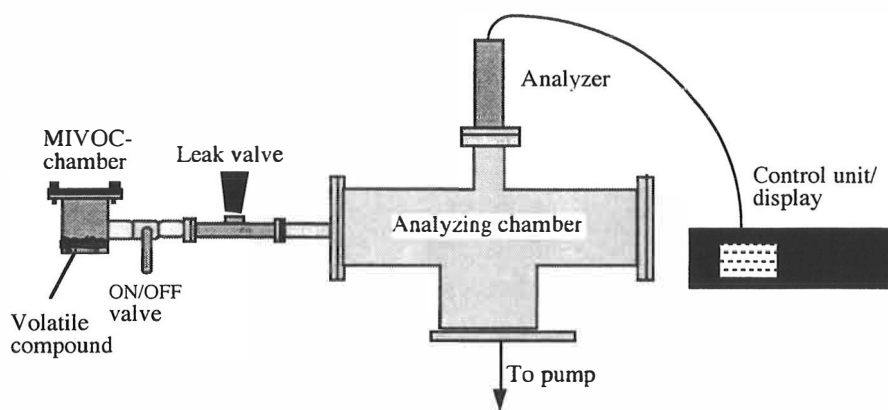


Figure 4.1: A schematic drawing of the MIVOC chamber connected to the analyzing chamber. The composition of the residual gas is measured by a Vacscan 100 F.

The residual gas is ionized by the hot filament of the analyzer. The pressure inside the analyzing chamber has to be lower than 1×10^{-5} mbar before switching the filament on. The ionized gas is guided to the quadrupole filter which separates the various ions according to their charge-to-mass ratio (q/A) and passes the single selected q/A to the

collector. The filtered ion beam is converted into a small electrical current which is amplified and measured to determine the partial gas pressure of the species selected by the quadrupole filter. The minimum pressure measurable by the VacScan 100F is 1×10^{-11} mbar.

4.2. The JYFL-ECR ion source

In the second phase of the development work the MIVOC chamber is connected to the second stage of the JYFL-ECR ion source [Ärj90]. The ECR ion source at the Accelerator Laboratory, University of Jyväskylä, is a modified copy of the RT-ECRIS [Ant86] at the National Superconducting Cyclotron Laboratory of Michigan State University in the USA. The JYFL-ECRIS is a two stage source where 6.4 GHz microwave power is fed axially into the first stage and radially into the second stage plasma chamber. The microwave transmitter has a maximum power of 3.35 kW. Figure 4.2 shows the construction of the JYFL-ECRIS in its present configuration.

Some improvements were made to the original design of the JYFL-ECR ion source: The 1st stage chamber was isolated from the second stage chamber in order to use a small negative voltage between them to supply electrons to the second stage plasma [Ärj93]. The Penning gauge of the second stage plasma chamber was removed and the ion gas feed line was connected to this port. This was found to decrease the consumption rate of the ion gas so that expensive isotopes can be used in a more economical way. The main parameters of the ion source are presented in table 4.1.

The mixing-gas which is used for ignition and maintenance of the plasma is fed into the first stage plasma chamber. The ion gas, used for the production of the ion beam, is fed directly into the second stage plasma chamber. In order to produce highly charged ion beams, more than 70 % of the total microwave power is fed into the second stage.

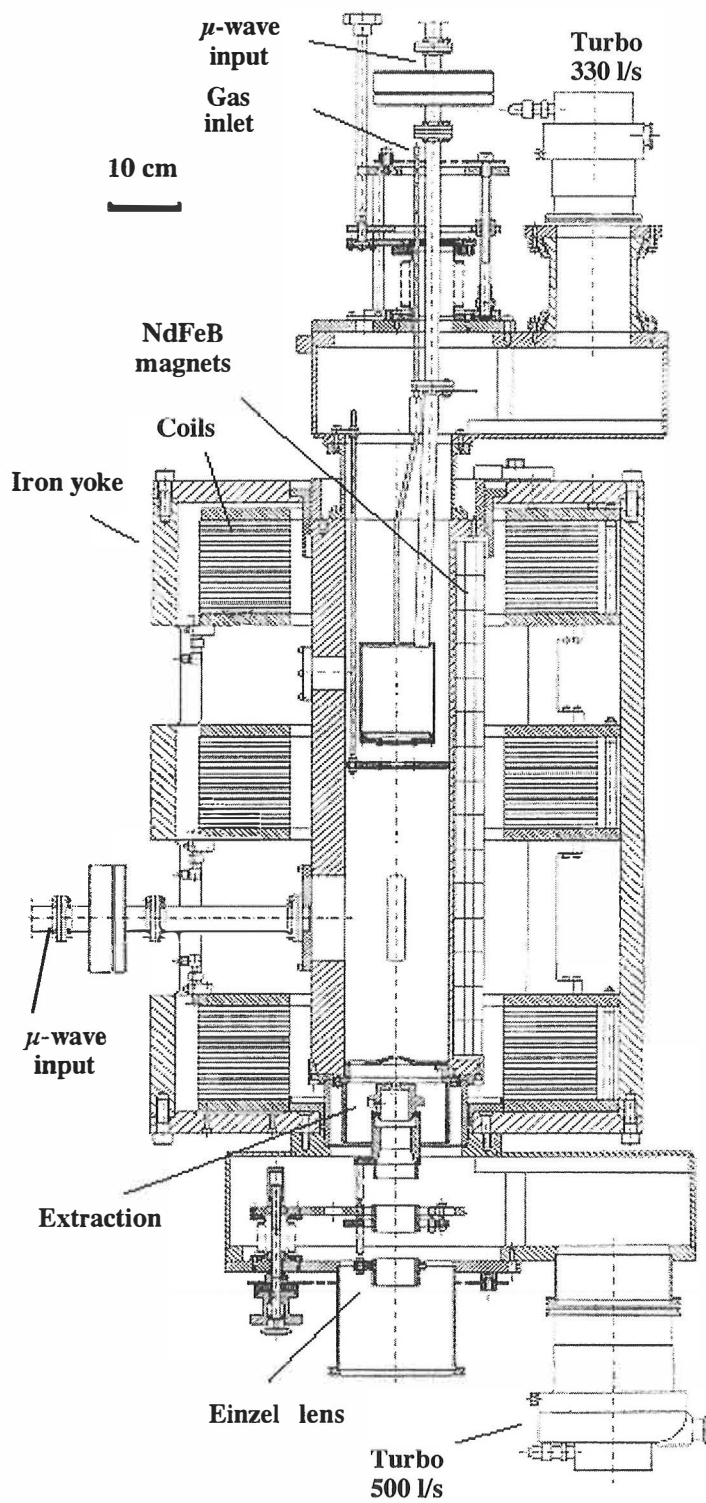


Figure 4.2: A side view of the JYFL-ECRIS

Main Stage: L = 40-50 cm (adjustable), $\phi = 14$ cm

Axial Magnetic Field:

Number of circular coils: 9

Coil dimensions: $R_i = 14.3$ cm, $\Delta R = 12.5$ cm, $\Delta z = 4.0$ cm

Coil construction: 3 double pancakes using 0.64×0.64 cm² conductor

Current range: 0-250 A ; nominal: 190 A

Nominal power consumption: 24 kW

Maximum obtainable B on axis: 0.38 T (@250 A)

Approximate mirror ratio range: 1.2 - 2.2

Hexapole Magnetic Field:

Neo ($B_r = 1.15$ T)

inner diameter 15.2 cm

pole width 5.1 cm

pole height 3.8 cm

pole length 76.5 cm

Max. field inside plasma chamber

- through hexapole bar center: 0.34 T

- through hexapole gap center: 0.27 T

Microvawe Power:

Total power of 3.3 kW at 6.4 GHz via power divider:

10 - 60 W into the first stage

50 - 150 W into the second stage.

High Voltage (maximum):

Main: 30 kV / 10 mA

Extraction: -15 kV / 20 mA

Vacuum pumping speeds:

Injection chamber 330 l/s

Extraction chamber 500 l/s

Basic vacuum 10^{-7} mbar.

Table 4.1: Constructional parameters of the JYFL-ECRIS.

4.3. The K-130 cyclotron

4.3.1. Maximum energy

The performance of the cyclotron determines the minimum charge state of the desired ion beam. The maximum extraction energy of the K130 cyclotron [Liu92] is

$$\frac{E_{\max}}{A} = K \left(\frac{q}{A} \right)^2 \quad (4.1)$$

where

$$K = \frac{(Br)^2 e^2}{2u}, \quad (4.2)$$

e is the elementary charge, u is the atomic mass unit, q is the charge state, B is the maximum magnetic field (1.76 T) and the extraction radius r is 0.94 m. The K value of the magnet of the cyclotron is 130 MeV.

A usual requirement for the energy of ions in low-energy nuclear physics is 5 MeV/u. In order to attain this value the minimum charge state of the ion has to be

$$q \geq 0.2A \quad (4.3)$$

For example, in the case of ^{84}Kr the minimum charge state to reach the energy of 5 MeV/nucleon is 17.

4.3.2. Resolution of analysing magnets and K130 cyclotron

Ions with same q/A ratio cannot be resolved by the analysing magnet of the ECR ion source. For example, in the case of $^{28}\text{Si}^{7+}$ and $^{16}\text{O}^{4+}$ the q/A ratio is 0.25, i.e. they overlap in the mass spectrum of the ECR ion source. The FWHM (Full Width at Half Maximum) resolution of the analysing magnet of the ECR ion source is measured to be 5 %.

Inside the cyclotron, the path of the accelerated ion in the magnetic field is very long leading to a very high resolving power. Using accurate masses, 27.9769u for ^{28}Si and 15.9949u for ^{16}O , the q/A difference between $^{28}\text{Si}^{7+}$ and $^{16}\text{O}^{4+}$ is 0.5%. Figure 4.3.

shows the ion mass spectrum obtained by tuning the magnetic field level of the cyclotron with the outermost trim coil. It is seen that ions of $^{28}\text{Si}^{7+}$ and $^{16}\text{O}^{4+}$ can be resolved in the K130 cyclotron. By using the silicon peak the FWHM resolution of the K130 cyclotron has been measured to be 0.3%. However, the mass difference between two important beams, $^{40}\text{Ar}^{8+}$ and $^{40}\text{Ca}^{8+}$, is only 0.005%. As a consequence, they cannot be resolved in the cyclotron.

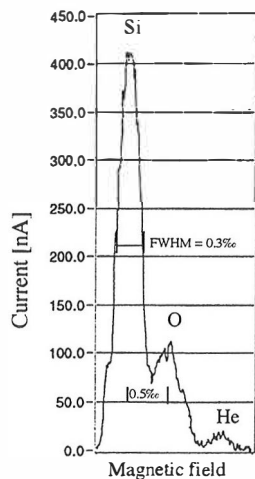


Figure 4.3: Resolution of the K130 cyclotron.

5. Optimizing of the JYFL-ECRIS for the production of metal ion beams

The first part of this section considers the methods for enhancing the intensity of highly charged ions. This study was carried out with gases. The second part deals with the gas feeding system developed in order to stabilize the gas feed rate. This system is necessary in the case of heavy ion beams obtained from solid materials when extremely stable ion beams are required.

5.1. Basic studies with gases with the JYFL-ECRIS

Several studies were performed with the JYFL-ECRIS with gases before the production of metal ion beams. Different mixing gases, the plasma cathode, and the aluminium foil insert have been used to improve the ion beam intensities. The effect of the gas mixing ratio and consumption rates of materials to be ionized were also studied. This kind of basic work has been necessary to understand the behaviour of the ion source and to determine the best conditions and tunings for the production of highly charged metal ion beams.

5.1.1. Methods to improve ion beam intensity with JYFL-ECRIS

5.1.1.a. Gas mixing

Gas mixing was the first method used to improve the ion beam intensity with the JYFL-ECR ion source. Different mixing gases and their ratios were investigated to understand the behavior of the ion source. As an example, figure 5.1 shows the enhancement of an argon ion beam intensity as a function of charge state when helium or nitrogen was used with the argon. The improvement of the intensity is compared to the argon beam without gas mixing.

Figure 5.1 shows that better results were achieved for the charge state up to Ar^{6+} , without gas mixing. In addition, helium was more effective for lower charge state argon compared to the nitrogen as a mixing gas. For charge states higher than $7+$, gas mixing was a quite effective method in improving the intensity of ion beams. The intensity of Ar^{8+} increased by factors of 1.7 and 2.2, and intensity of Ar^{9+} increased by factors of 2.6 and 4.0, when helium or nitrogen were used as a mixing gas. The improvement obtained by gas mixing tends to increase as a function of the charge state.

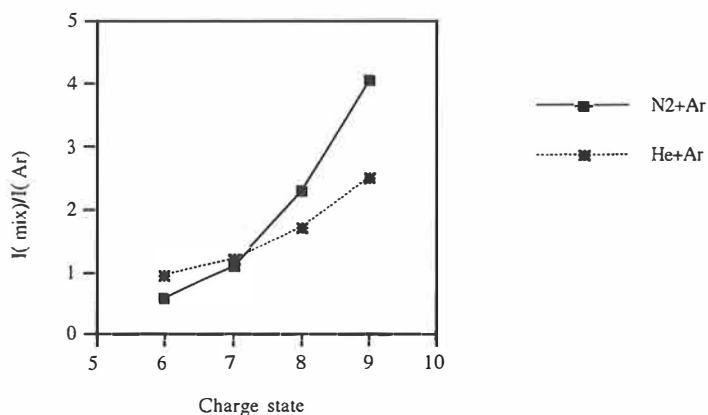


Figure 5.1: Relative argon ion beam intensity $I(\text{mix})/I(\text{Ar})$ as a function of charge state. Here $I(\text{mix})$ refers to the intensities of argon ions with gas mixing and $I(\text{Ar})$ refers to intensities without gas mixing.

5.1.1.b. The plasma cathode method with the gas mixing

In 1993 the first stage chamber of the JYFL-ECRIS was isolated from the second stage chamber in order to use the plasma cathode method. Several experiments were performed to determine the influence of the negative voltage. The efficiency of this method was found to depend critically on the tuning of the ECR ion source. Figure 5.2. shows the enhancement of the $^{58}\text{Ni}^{10+}$ ion beam as a function of the plasma cathode voltage.

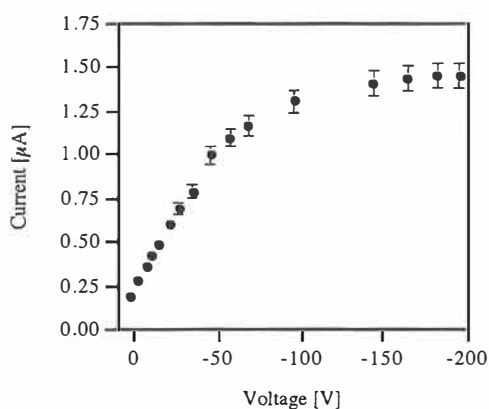


Figure 5.2: The behaviour of the ion beam intensity of $^{58}\text{Ni}^{10+}$ as a function of plasma cathode voltage.

For example, after accurate gas mixing and tuning, the improvement using the plasma cathode for the Ar^{8+} ion beam is normally of the order of 10 - 20 %. In the case of Ar^{9+} , slightly better improvements can be achieved - however, rarely higher than 50 %. The intensity of the ion beam usually improved quite steeply when the plasma cathode voltage was increased from 0 V to -100 V. Beyond -100 V, the effect became more gradual and saturation was reached with a bias voltage of less than -200 V.

5.1.1.c. The plasma cathode and the gas mixing method with the aluminium foil liner

In autumn 1996, an aluminium foil liner was installed inside the second stage plasma chamber of the JYFL-ECRIS. The oxidized surface of the aluminium foil behaves as a source of electrons and increases the electron density in the plasma (table 3.1). During this experiment, the plasma cathode method was not used. Argon was fed into the second stage plasma and the current for each charge state was maximized and measured. Nitrogen was used as a mixing gas. The result of these experiments was that the same ion currents were achieved with the foil as with the plasma cathode method.

The aluminium foil was next tested with the plasma cathode method. No improvement was noticed in ion current as a function of the bias voltage. This may indicate that, the electron emission yield from the aluminium foil via electron impact is adequate to reach sufficient electron density in the second stage plasma, i.e. optimal $n_e \tau_i$ conditions are reached. As a consequence, the plasma cathode is not needed when aluminium foil is used. In addition, the foil acts as protection against the contamination of the plasma chamber walls, and it can easily be replaced during a maintenance period.

The effect of gas mixing was also investigated with the aluminium foil. Since the optimal $n_e \tau_i$ condition is achieved already with the aid of aluminium foil the use of the gas mixing should not increase the current of ion beams. However, as figure 5.3 shows, surprisingly high improvement of the ion beam current was achieved. Mixing gases nitrogen and oxygen turned out to be very effective. In the case of helium, intensities of charge states of argon decreased. Possibly, optimal tunings were not found.

As a conclusion, the electron density of the plasma can be increased either with the aluminium foil or with the plasma cathode. No additional improvement was obtained

using both methods at the same time. The gas mixing method enhances the ion beam intensity when used together with either the plasma cathode or the aluminium foil.

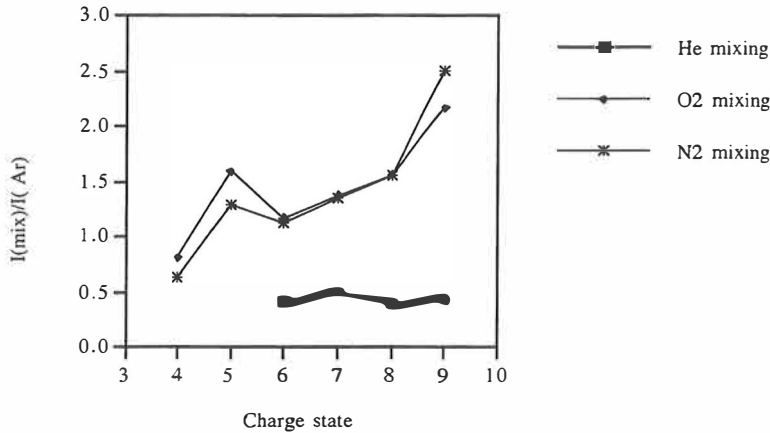


Figure 5.3: The increase of the argon ion beam as a function of charge state when different mixing gases were used. An aluminium foil liner was used in the second stage plasma chamber. In the spectrum Ar^{5+} is overlapped by O^{2+} ions.

5.1.2. The gas consumption rate and the gas mixing ratio

The object of this study was to estimate the material consumption rate of the ECR ion source and the mixing ratio of the mixing and ion gas in the second stage plasma. The values of these quantities were calculated from the measured values of the gas pressures inside the ion source and the known pumping speeds. The output values were calculated with a specially developed calculator based on the Excel spreadsheet. Table 5.1 shows the layout, i.e. the input and output values, of the calculator. The calculator has turned out to be a very helpful tool in the estimation of the operation of the ECR ion source.

The calculator is designed for a two stage ECR ion source where the mixing gas is fed into the first stage plasma chamber and the ion gas directly into the second stage. Both vacuum chambers are pumped separately by turbo molecular pumps at the pumping speeds of 330 l/s and 500 l/s for the first and the second stage, respectively. The conductance between the pumps and the plasma chambers has been taken into account. The structure and the position of the pressure gauges and the vacuum pumps can be seen from figure 4.2.

Gas consumption rate and gas mixing ratio calculator:

Pressure input values		
1st. stage: N₂		
Pressure without gas feed:	0.1	E-6 mbar
Plasma OFF pressure:	4	E-6 mbar
Atom mass of mixing gas:	28	amu
Calibr. factor of mixing gas:	1	
2nd. stage: Ar		
Pressure without gas feed:	0.1	E-6 mbar
Plasma OFF pressure:	0.58	E-6 mbar
Without ion gas feed:	0.46	E-6 mbar
Atom mass of ion gas:	40	amu
Calibr. factor of ion gas:	1.2	

Element:	Calib. fact:
Argon	1.25
Helium	0.17
Hydrogen	0.44
Krypton	2
Neon	0.24
Nitrogen	1
Oxygen	1

Calibr. factor of calculator 0.43
 Temperature: 292 K

Pumping speeds (input values)			Pumping speeds (output values)		
1st stage:			first stage:		
Pumping speed of pump:	330	l/s	Conductance of pump=	382	l/s
Lenght of pumping line:	15	cm	Pumping speed=	177	l/s
Diameter of pumping line:	9.5	cm			
2nd stage:			second stage:		
Pumping speed of pump:	500	l/s	Conduct. for mixing gas=	1300	l/s
Lenght of pumping line:	12	cm	Conduct. for ion gas=	1087	l/s
Diameter of pumping line:	15	cm	Pump. speed of mix. gas=	361	l/s
			Pump. speed of ion gas=	343	l/s
Injection line:					
Pump. speed of mixing gas =	38	l/s			
Pump. speed for ion gas =	33	l/s			

RESULTS:

Consumption rate of:		
mixing gas=	1.4	cm³/h
ion gas=	0.06	cm³/h
mixing ratio=	22	%

Table 5.1: The calculator for the estimation of the gas consumption rate and the gas mixing ratio in the operation of the JYFL-ECRIS.

Pressure input values are measured after the ECR run in “plasma-OFF”-mode as follows: pressures in the first and second stage and pressure in the second stage without ion gas feed. The basic vacuum of the ECR ion source has to be also known, i.e. pressure without ion and mixing gas feed. The molecular mass of the particles in the plasma has to be given in order to determine the pumping speeds. The calibration factor [Bal88] of the Penning gauge for different elements has been taken into account. The true pressure can be calculated using equation (5.1)

$$\text{True pressure} = \frac{\text{meter reading}}{\text{gas calibration factor}} \quad (5.1)$$

The calibration factor of the calculator was determined by using a vacuum chamber of 0.5 l filled with nitrogen or hydrogen. The gas was allowed to flow into the ECR ion source via an accurate leak valve during the normal ECR operation. The decrease of the pressure was measured as a function of time by a capacitive sensor. As a result, the hydrogen and the nitrogen consumption rates were measured to be 34 cm³/h and 1.4 cm³/h, respectively. The corresponding values obtained by the calculator are 79 cm³/h and 3.2 cm³/h, respectively. The difference between the calculated and measured values is mainly caused by the contamination of the Penning gauge. Using the above mentioned values, the calibration factor of the calculator for hydrogen and nitrogen were 0.43 and 0.43. As a consequence, the factor of 0.43 has been used. The same calibration factor with different gases indicates that most probably all parameters have been taken into account in the calculator.

<i>Element</i>	<i>q</i>	<i>Consumption rate [cm³/h]</i>	<i>Mixing ratio</i>	<i>Mixing gas</i>
<i>H2</i>	1	34	*	*
<i>He</i>	1	35	*	*
	2	8.3	*	*
<i>N2</i>	Ar8+	1.4	95%	**
<i>36Ar</i>	8	0.010	4.8%	N2
<i>40Ar</i>	7	0.13	39%	N2
<i>40Ar</i>	8	0.078	27%	N2
<i>40Ar</i>	9	0.059	22%	N2

Table 5.2: Consumption rates and mixing ratios calculated by the calculator. The second column shows the charge state of the element the ECRIS was optimized for. Single asterisk denotes when the gas mixing was not involved. Double asterisks denote when the element was used as a mixing gas.

Table 5.2 shows an example of the results obtained with the calculator. The second column shows the charge state the ion beam was optimized for. In the case of the $^{36}\text{Ar}^{8+}$ ion beam production the consumption rate of nitrogen was $1.4 \text{ cm}^3/\text{h}$. This value is typical for the mixing gas. Consumption rates of ion beams of a low charge state can be even tens of cm^3/h when high intensity is required - for example in the case of H^+ and He^+ ion beams. When gas mixing is used and the ion gas is fed directly into the second stage plasma a consumption rate of the ion gas of less than $0.1 \text{ cm}^3/\text{h}$ is usually achieved.

Table 5.2 shows that only $0.01 \text{ cm}^3/\text{h}$ of argon was used when an $^{36}\text{Ar}^{8+}$ ion beam was produced. At that time, the ion gas feed rate was limited to the lowest value sufficient to reach the required ion beam intensity on the experimental target (after the K130 cyclotron). Table 5.2 shows that the consumption rate of the ion gas tends to decrease as a function of the charge state, i.e. the mixing ratio of the ion gas tends to decrease as a function of higher charge state.

5.1.3. Gas consumption rate as a function of charge state

The consumption rate of argon was studied as a function of the charge state when nitrogen was used as a mixing gas. Figure 5.4 shows the results obtained when the ion beam intensity was maximized for the charge states of Ar^{7+} , Ar^{8+} and Ar^{9+} by changing the gas mixing ratio. Other parameters like μ -wave power and magnetic field were kept constant. In the same figure, the consumption rates of nitrogen are presented.

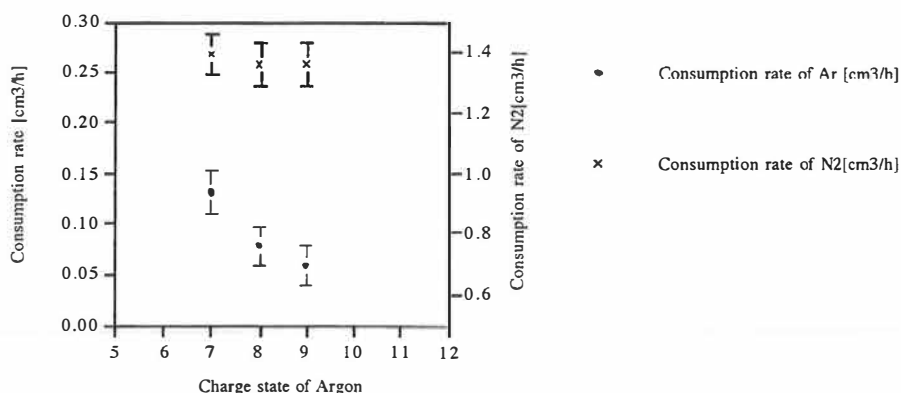


Figure 5.4: The consumption rates of argon and nitrogen as a function of the argon charge state. Nitrogen was used as a mixing gas.

The values obtained have been calculated with the aid of the above mentioned calculator. Note the different scales for the argon and nitrogen consumption rates. In this experiment the only variable parameter was the argon consumption rate which affected the mixing ratio, i.e. the parameter n_0 in the second stage plasma decreased with increasing charge state. The intensity of highly charged argon ions increased slightly (<10 %) when the gas consumption rate was decreased as a function of the charge state.

The rate of the change of the ion density in the ECR ion source plasma at the charge state q was given by equation (2.2). In order to enhance the production rate of highly charged ions, losses have to be reduced or the ionization efficiency has to be increased. Figure 5.4. showed that the material consumption rate decreases as a function of the charge state when the gas mixing ratio was optimized. The neutral gas feed rate was decreased which probably decreases the charge exchange reactions between the neutrals and highly charged ions. This means that losses due to the third bracket term, $\sigma_{q,q-1}$, were reduced. Another possible explanation is that the amount of the electrons decreases when the gas feed rate is decreased. As a consequence the energy per electron increases leading to a more effective ionization of highly charged ions.

As equation 2.4. shows, the charge exchange cross-section increases as a function of the charge state and decreases as a function of the ionization potential of the target atom. The ionization potential of helium is very high and it should thus be very effective as a mixing gas. However, experiments have shown that nitrogen and oxygen are more efficient as mixing gases. One possible explanation can be found from figure 3.3, i.e. the cooling of the heavy ions is more efficient with nitrogen and oxygen.

5.1.4. Studies of ionization efficiencies

In this measurement, the consumption rate of the gas and the total extracted ion current were measured in order to determine the ionization efficiencies of mixing and ion gases. In the first part, nitrogen was studied without the gas mixing. During the experiment, the magnetic field and microwave power were kept constant. Therefore, the only free parameter was the gas feed rate which was calculated using the calculator described in section 5.1.2. Two different gas feed rates of nitrogen were tested.

Figure 5.5 shows the beam intensity of nitrogen as a function of the charge state. The consumption rates of nitrogen of $0.28\text{cm}^3/\text{h}$ and $0.22\text{ cm}^3/\text{h}$ were used which corresponds to 1.9×10^{15} molecules/s and 1.5×10^{15} molecules/s, respectively. The gas

consumption rate of the first stage was ignored. As figure 5.5 shows, the intensity of highly charged ions decreased when the gas feed rate was increased.

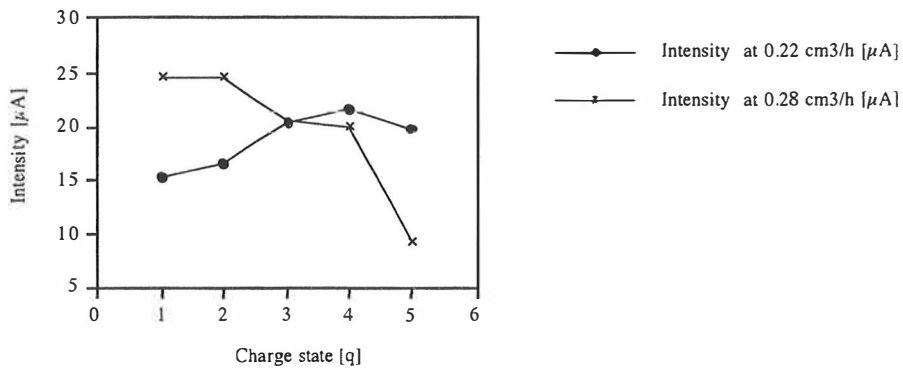


Figure 5.5: The intensity of nitrogen as a function of the charge state. Filled circles and crosses denote nitrogen feed rates of 0.22 cm³/h and 0.28 cm³/h, respectively, into the second stage chamber.

The currents of the charge states from N_2^+ to N^{5+} were determined from the mass spectrum obtained. The total molecular nitrogen flow of these charge states was calculated to be 2.3×10^{14} molecules/s and 1.7×10^{14} molecules/s. Using the values obtained, the particle ionization efficiencies are calculated to be $(12.1 \pm 0.5)\%$ and $(11.6 \pm 0.5)\%$, respectively. Regardless of the different charge state distributions (Fig. 5.5.) nearly constant ionization efficiencies were measured. At these conditions almost 90 % of the gas that was fed into the ion source was evacuated by the turbo molecular pumps.

The particle ionization efficiency of nitrogen was next tested with the argon mixing. A constant nitrogen gas feed rate of 0.22 cm³/h was used and argon was mixed into the nitrogen plasma to maximize the current of the Ar^{8+} beam. Intensities of different charge states were then measured. Figure 5.6 shows the intensities of the different argon and nitrogen charge states as a function of the charge state. The currents of nitrogen charge states obtained without the gas mixing are shown for comparison.

The intensities of highly charged nitrogen ions decreased considerably, when argon was added into the plasma. For example, the intensity of N^{5+} beam diminished from 19.7 μA to 0.7 μA , i.e. by a factor of 28. At the same time the intensity of N^+ increased. In collisions between the heavier and lighter ions, the kinetic energy of the lighter ions will increase and their confinement time will shorten. As a consequence, the lifetime of the mixing gas ion is too short to achieve a high charge state.

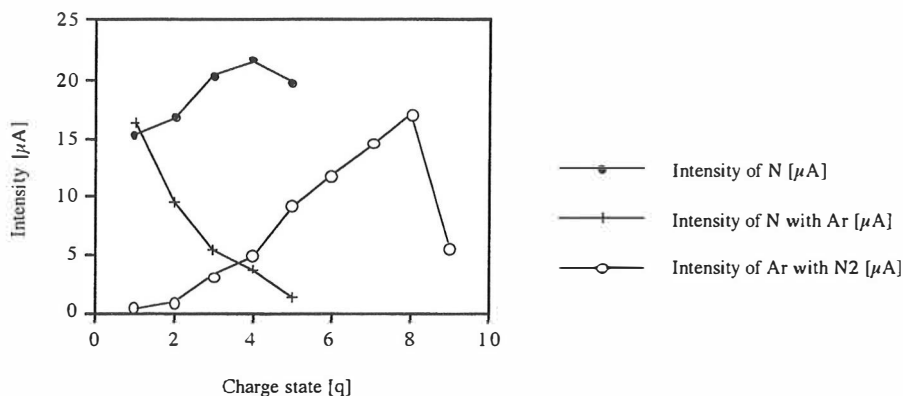


Figure 5.6: The intensity of argon and nitrogen as a function of the charge state. Filled circles denoted when pure nitrogen was used. Open circles and crosses corresponds to argon and nitrogen currents, respectively

With the aid of the consumption rate calculator the consumption rate of argon was calculated to be $0.10 \text{ cm}^3/\text{h}$, which corresponds to 7.0×10^{14} atoms/s. The gas mixing ratio was 32 % of argon in the plasma. Total flow rates of nitrogen and argon were measured to be 9.3×10^{13} molecules/s and 9.0×10^{13} atoms/s, respectively. Using these values, the particle ionization efficiencies of argon and nitrogen was calculated to be $(12.9 \pm 0.5)\%$ and $(6.2 \pm 0.5)\%$, respectively. This experiment showed, that the confinement of nitrogen gets worse when it was used as a mixing gas with the heavier argon. One explanation can be found from section 3.1.2, i.e. due to the collisions the velocity of the mixing gas element increases. As a consequence, its probability to leave the plasma and be evacuated by the pumps increases.

5.2. The gas feeding system used with the JYFL-ECRIS

5.2.1. Introduction

A special gas feeding system was developed for use with the JYFL-ECR ion source to increase the stability of the ion beams. In the operation of an ECR ion source, the parameters related to the tuning of the source must remain constant to ensure production of stable ion beams. Especially in the case of highly charged ions, the beam current is very sensitive to any changes in plasma parameters.

The gas pressure inside the plasma chamber is one of the most critical parameters. Even a small change in pressure may strongly affect the extracted ion current. This is

demonstrated in figure 5.7, which shows the current of a O^{5+} beam as a function of gas pressure inside the main plasma chamber. Furthermore, direct control of the small gas flow has turned out to be both cumbersome and unreliable.

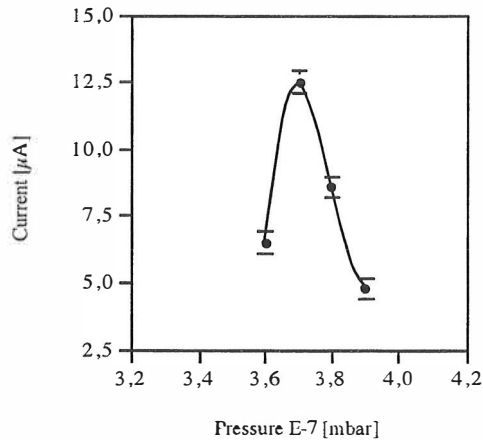


Figure 5.7: The ion current of O^{5+} as a function of gas pressure inside the plasma chamber.

In order to overcome this problem, and to keep plasma conditions constant, the gas pressure at the inlet of the ECR ion source must be stabilized. This was accomplished by using a two-tank system with a low-conductance capillary tube between the two tanks. The tank system is then connected to a leak valve at the gas inlet of the source. Since the gas mixing method is used for production of highly charged ions, two separate tank systems are used with the JYFL-ECRIS - one for mixing gases and one for ion gases. However, in case of an expensive, low pressure gas the new gas feeding system is by-passed and the bottle is directly connected to the leak valve of the ion gas line.

5.2.2. Description of the new gas feeding system and its operation

Figure 5.8 shows a schematic drawing of the new gas feeding system. It consists of two vacuum tanks with pressure meters, four valves and two separate filling tubes between the tanks. Tank 1 is connected to the gas bottle and tank 2 to the leak valve by 6 mm stainless steel tubes. Tank 1 works as a buffer that enables the pressure of tank 2 to be strictly controlled. The operation is as follows: The evacuated tank 1 and tank 2 are manually filled from a gas bottle to a few hundred mbar. The manual on/off valve between the tanks is closed and pressure in tank 1 is further raised, to a pressure of less than 1000 mbar. From tank 2 the gas is delivered into the source through a leak valve.

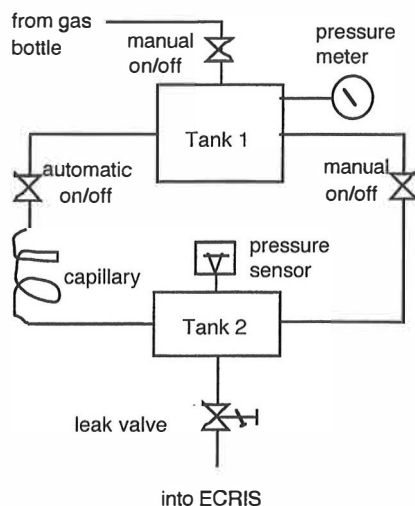


Figure 5.8: Principle of the new gasfeeding system at the JYFL-ECRIS.

The stability of the system is based on a constant pressure in tank 2, i.e. the inlet pressure of the leak valve remains constant. When the accurately monitored pressure in tank 2 falls below a preset value, an automatic on/off-valve allows the gas from tank 1 to flow into tank 2 through a teflon capillary. The low conductance of the capillary ensures a well controlled flow into tank 2 and eliminates overloads. The pressure in tank 1 is measured by a rough and low-cost Bourdon gauge, while the pressure in tank 2 is measured with an accurate capacitive sensor.

5.2.3. Development of the gas feeding system

5.2.3.a. Theoretical studies

From figure 5.7 it can be estimated that a pressure fluctuation of $\approx 0.5\%$ may cause an intensity drop of $\approx 5\%$ in the O^{5+} beam. Based on this, a pressure of 200 mbar was chosen for tank 2. This value should fluctuate only within $\pm 0.1\%$, i.e. ± 0.2 mbar. These values were used as a starting point in the design of the gas feeding system described above. The design included determination of the tank volumes, and of the length and diameter of the capillary. All these parameters should fit the control sequence of the main control system [Ärj90] of the source.

With a capacitive sensor the accuracy of the tank 2 pressure measurement is ± 0.1 mbar and a reading is taken 10 times per second. Based on earlier experience in gas consumption of the source, the tank volumes were fixed to 1 litre for tank 1 and 0.5 liters for tank 2. From these values it can be estimated that the pressure inside tank 2

should increase by 1 mbar per second, i.e. with a flow rate of 0.5 mbar l/s, in order to keep the pressure in use within ± 0.1 %. The length and diameter of the required capillary were estimated theoretically [Fon86, Rot82] and finally verified experimentally.

In order to determine the conductance of the capillary it is necessary to know the state of the flow through it. As mentioned earlier, the change in gas pressure in the gas feeding line was determined to be lower than ± 0.2 mbar and the maximum throughput of the capillary Q_{\max} lower than 0.5 mbar l/s, i.e. $0.5 \text{ cm}^3/\text{s}$ (NTP). The limit between the molecular, intermediate and viscous state can be defined with the aid of the Knudsen number,

$$N_K = \left(\frac{D}{\lambda} \right), \quad (5.2)$$

as follows:

$N_K > 110$	viscous flow
$1 < N_K < 110$	intermediate flow
$N_K < 1$	molecular flow,

where λ is the mean free path of the molecule and D is the diameter of the capillary. For the capillaries with diameters of 0.3 mm and 0.8 mm, the Knudsen numbers were calculated to be 4690 and 12500, respectively.

The limit between the turbulent and laminar flow can be defined with the aid of the Reynolds number, N_R . It is a dimensionless quantity expressed by

$$N_R = \delta v D / \eta, \quad (5.3)$$

where δ is the gas density (1.17 kg/m^3 for air), v is the average flow velocity and η is the coefficient of viscosity ($1.71 \times 10^{-5} \text{ kg/m}\cdot\text{s}$ for air). The average flow velocity v [m/s] through the capillary can be solved by using the equation

$$v = \frac{Q_{\max}}{A}, \quad (5.4)$$

where the maximum throughput of the capillary Q_{\max} (NTP) is in $[\text{m}^3/\text{s}]$ and the cross section of the capillary hole, $A = \pi r^2$, is in $[\text{m}^2]$. Using equations (5.3) and (5.4), the Reynolds numbers for capillaries with diameters of 0.3 mm and 0.8 mm were calculated to be 145 and 54, respectively. The flow will be laminar if $N_R < 1100$.

With the aid of the Knudsen and Reynolds numbers, the flow is found to be viscous and laminar. In this state of flow, the conductance C [m³/s] of a long cylindrical pipe [Roth82] can be presented as

$$C = \frac{\pi \cdot D^4}{256 \cdot \eta \cdot L} \cdot (P_1 + P_2) \cdot 100, \quad (5.5)$$

where P_1 and P_2 [mbar] are pressures at the inlet and output of the capillary, and D [m] and L [m] are diameter and length of the capillary, respectively. The constant 100 is used to convert mbar to Pa. The throughput of the capillary is obtained by using equation,

$$Q = C \cdot (P_1 - P_2). \quad (5.6)$$

5.2.3.b. Experimental studies

In the experiments, air was allowed to flow from atmosphere into the evacuated test vacuum chamber of 19.6 cm³ in volume while the pressure was measured as a function of time using a capacitive sensor. Time behaviour of the pressure was registered by a PC computer. Figure 5.9 shows results when teflon capillaries with inner diameters from 0.3 mm to 0.8 mm were tested. Measurement of the 0.3 mm capillary with a microscope gave an average inside diameter of 0.34 mm. Lengths of the capillaries were the same, $L=60$ cm.

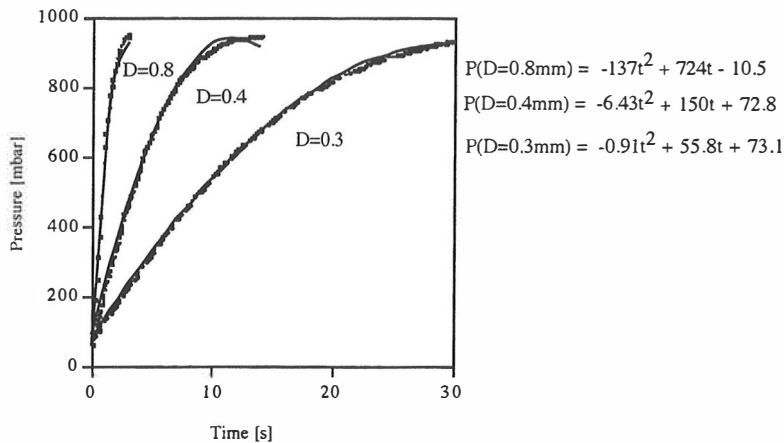


Figure 5.9: Pressure of the test vacuum chamber as a function of time when air was allowed to flow into the chamber through different capillaries. Inner diameters of the capillaries were 0.3 mm, 0.4 and 0.8 mm and lengths were 60 cm. The first curve from the left corresponds to the capillary of 0.8 mm in diameter.

The polynomial curve fits for the different capillaries are presented on the right hand side of figure 5.9. By using the curve fits, the rate of the pressure change can be defined at any moment. In this work the rates were defined at the point of 200 mbar which was chosen as the constant pressure to be maintained in tank 2.

From the curve fits in figure 5.9 the slopes of the curves at 200 mbar were determined for the 0.3 mm and 0.8 mm capillaries. These corresponded to throughputs of 1.0 mbar l/s and 12.5 mbar l/s, respectively. To ensure the slow filling of tank 2 the capillary with diameter of 0.3 mm was chosen for further experiments. In the next phase pressure behaviour in the test vacuum chamber was measured as a function of time for the chosen 0.3 mm capillaries with different lengths. The results are shown in figure 5.10.

By using the equations in figure 5.10 the rate of pressure change, at the point $P = 200$ mbar, can be found. At that same point the throughput of the capillary is obtained from the equation

$$Q = (2at + b)V, \quad (5.7)$$

where $(2at + b)$ is the time derivative of the appropriate fitted polynomial in figure 5.10 and V is the volume of the vacuum chamber.

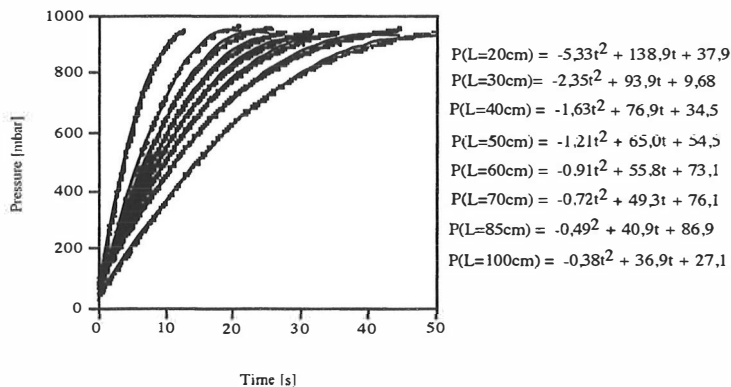


Figure 5.10: Pressure in the test vacuum chamber as a function of time for 0.3 mm capillaries with different lengths. Length of the capillary increases from left to right.

In figure 5.11, both theoretical and experimental throughputs are presented for eight capillaries with different lengths. The theoretical and experimental curves are calculated with the aid of equations (5.6) and (5.7), respectively. With the requirement of 0.5

mbar l/s the theoretical and experimental lengths of the capillaries were defined to be 113 cm and 140 ± 10 cm, respectively.

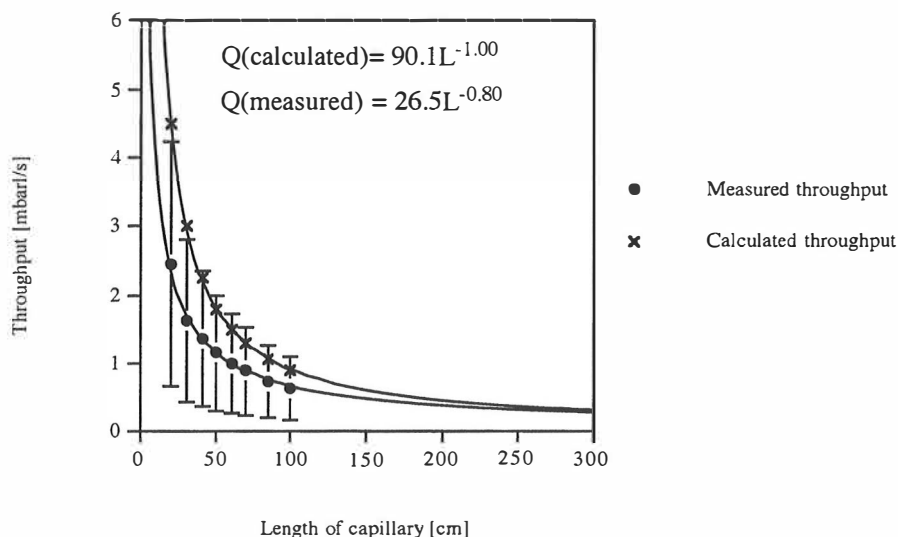


Figure 5.11: Throughput of the 0.3 mm diameter capillary as a function of length of the capillary. The measured and calculated curves are presented.

To restrict the throughput to lower than 0.5 mbar l/s, a 0.3 mm capillary of at least 150 cm is required. The viscosity factor of air is about twice that of hydrogen. As a final result, the capillary of $L=300$ cm fulfills the initial requirement for all gases. In figure 5.11 an extrapolation of the experimental and theoretical curves up to 300 cm gives practically equal results.

The new gas feeding system for the JYFL-ECRIS has been used since 1995. It has turned out to be very useful and reliable. In a normal ECR run the pressure in tank 1 is ≈ 700 mbar and in tank 2 it is 200.0 mbar. The control system admits more gas into tank 2 through the capillary when the pressure is below the preset value. Otherwise the on/off valve between the tanks is closed. Proceeding this way the pressure inside tank 2 is within 199.5 mbar and 200.4 mbar for hydrogen. For heavier gases the pressure variation is even less. This ensures very stable ion beams without further tuning.

In normal ECRIS runs, filling of tank 1 in the buffer gas line where the gas consumption is the largest (5-10 times that of the ion gas) is required only once a week. Filling can be done without interruption in the source operation. A similar system is applied to the ion gas line, too. There, however, in case of expensive, sub-atmospheric

pressure gases the gas is directly fed from a gas bottle into the leak valve. Using the described gas handling system, the beams from the JYFL-ECRIS have appeared stable during long-term (>1 week) experiments. As an example, during a nuclear physics experiment of two weeks, no adjustment of the ECR ion source was needed. Table 5.3 summarizes the parameters which are used in the new gas feeding system when applied to the ion beam production with the JYFL-ECRIS.

<u>Item</u>	<u>Quantity</u>	<u>Unit</u>
Volume of tank 1	1	litre
Volume of tank 2	0.5	litre
Pressure in tank 1	200-1000	mbar
Pressure in tank 2	200.0 ± 0.2	mbar
Length of capillary	300	cm
Diameter of capillary	0.34	mm
Conductance of capillary	~3x10 ⁻⁴ (for nitrogen)	l/s
Gas consumption	0.03 - 8	μbar l/s
Control cycle	0.1	s

Table 5.3: Specifications of the gas feeding system.

6. The MIVOC method

The standard technique for the production of an ion beam from most metals involves heating the feed material in order to raise its vapour pressure to a sufficient level. These methods are characterized by a more or less violent vaporization of solid or molten materials at or near high vacuum conditions. This tends to lead to contamination when the hot metal vapour condenses on the cold walls of the ion source. In order to overcome at least some of these problems a new method was developed. The objective of this work was to *produce a metal ion beams without heating*.

The first part of this chapter considers the physical basis of producing metal ion beams from volatile compounds. The second part deals with the experiments carried out to understand the behaviour of the compounds used and to maximize the intensity of highly charged metal ion beams produced from these compounds.

6.1. The physical basis of the MIVOC method

The MIVOC method is based on the fact that an ECR ion source requires a very small quantity of the ion gas. The gas consumption experiments showed (Section 5.1.2) that the total consumption rate of gas (ion+mixing gas) is on the order of 1 cm³/h (NTP) which corresponds to 3×10^{-4} mbar l/s. For ionization of heavier elements, for example argon and krypton, nitrogen or oxygen is typically used as a mixing gas. Under such conditions consumption rate of the ion gas is measured to be on the order of 0.1 cm³/h, i.e. 3×10^{-5} mbar l/s. As was shown in section 5.1.3. the consumption rate of the ion gas decreases as a function of the charge state.

In order to produce a metal ion beam, a volatile compound containing the metal element has to be found. The evaporation rate of the compound has to correspond to the consumption rate of the ion gas, i.e. 0.1 cm³/h NTP. The element in question has to be the heaviest atom in the compound in order to produce as intensive ion beam as possible with the lowest material consumption rate. The amount of other elements in the compound has to be as low as possible to minimize the feed rate of undesired material into the plasma.

6.1.1. Minimum vapour pressure required

The flow rate of a gas can be defined as the number of molecules passing through a cross section of the transmission line per second. The direction of the molecule flow (or gas flow) is towards the decreasing pressure, i.e. at zero pressure gradient the net flow through the cross section is zero. The flow through a cross section increases when the pressure gradient increases. The conductance is a function of the molecular mass, temperature, and the shape, diameter and length of the transmission line. The flow rate of the gas through the gas feeding system can be calculated when its conductance is known.

Usually the vapour pressure of a solid compound is very low at room temperature and consequently the molecular theory of conductance can to be used to define the conductance of each component of the gas feeding system [Rot82]. The total conductance of a system of several elements in series can be found with equation (6.1)

$$\frac{1}{C_{\text{tot}}} = \frac{1}{C_1} + \frac{1}{C_2} + \dots + \frac{1}{C_n} \quad (6.1)$$

The ion gas feed rate has to be equal to the consumption rate of the ECR ion source, i.e. on the order of 0.1 cm³/h. The operating pressure in the source plasma chamber is in the range of 10⁻⁷ mbar. As a consequence, the minimum required vapour pressure inside the MIVOC chamber can be calculated with the aid of equation (6.2) [Rot82],

$$C = Q/(P_{\text{sat}} - P_{\text{ecr}}) \approx Q/P_{\text{sat}} \quad (6.2)$$

where,

C = conductance of the gas feeding system [l/s],

Q = throughput of vapour [mbar l/s],

P_{sat} = saturated vapour pressure inside the MIVOC chamber [mbar],

P_{ecr} = operating pressure of ECRIS [mbar].

A calculation of the conductance for the present gas feeding system between the MIVOC chamber and the JYFL-ECR ion source shows the gas control valve to be the limiting section of the system with its maximum conductance of ≈ 0.04 l/s. Using the above mentioned ion gas throughput of 3x10⁻⁵ mbar l/s and inserting these two values into equation (6.2), the minimum required vapour pressure of a compound at room temperature is calculated to be

$$P_{\text{sat}} \approx 1 \times 10^{-3} \text{ mbar}. \quad (6.3)$$

The above mentioned requirements concerning the minimum vapour pressure can be lowered by increasing the conductance of the transmission line. These will, of course, increase the number of suitable compounds and make it possible to use the MIVOC method for more elements. However, higher requirements will be placed upon the purity and dryness of the compounds.

6.1.2. Saturated vapour pressure

In compounds, molecules are bound to each other via intermolecular forces. The average thermal energy of the molecules is generally not high enough to separate and free them at room temperature. However, due to the Gaussian type energy distribution individual molecules are able to leave the surface of the compound.

If the compound is in a vacuum chamber, the vapour pressure rapidly reaches its value of saturation. The vapour pressure depends on the nature of the compound and on the ambient temperature. In saturation, a dynamic equilibrium is reached between the surface and the vacuum chamber volume which means that the net number of the molecules in the gaseous state is constant.

Vapour pressures of different chemical compounds at room temperature are frequently not given or not known. Numerous equations and correlations for estimating the saturated vapour pressure can be found from the literature. The equations relating the vapour pressure as a function of the temperature are the most commonly derived by integration of the Clausius-Clapeyron equation [Lym90]

The method mainly used for the pressure estimation in this work is a modification of the Watson correlation [Lym90]. The estimation of the vapour pressure at some temperature using the Watson correlation (Eq. 6.4) requires information on the boiling point, T_b .

$$\ln P_{vp} \approx \frac{\Delta H_{vb}}{\Delta Z_b R T_b} \left[1 - \frac{(3 - 2T_{\rho b})^m}{T_{\rho b}} - 2m(3 - 2T_{\rho b})^{m-1} \ln T_{\rho b} \right] \quad (6.4)$$

where $T_{\rho b} = T/T_b$, $\Delta H_{vb} = T_b K_F (8.75 + R \ln T_b)$. K_F can be found from the tables [Lym90] and m depends on the physical state at the temperature of interest. For solids the following values are recommended:

$$T_{\rho b} > 0.6; m = 0.36$$

$$0.6 > T_{\rho b} > 0.5; m = 0.8$$

$$T_{\rho b} < 0.5; m = 1.19.$$

The error of this method is about 2-3 % at the pressure range of (10-1000) mbar, 40 % at the pressure range of (10^{-3} - 10) mbar and 50 % at the pressure range of (10^{-7} - 10^{-3}) mbar.

Figure 6.1 shows the calculated saturation vapour pressure of ferrocene, $\text{Fe}(\text{C}_5\text{H}_5)_2$, as a function of temperature. At room temperature, the vapour pressure is of the order of 1×10^{-3} mbar. As a consequence, ferrocene fulfills the requirement concerning the minimum vapour pressure required for the MIVOC method (Eq. 6.3). Ferrocene was used for the production of the first MIVOC beam. It is also used as a reference compound when new MIVOC compounds are sought and tested.

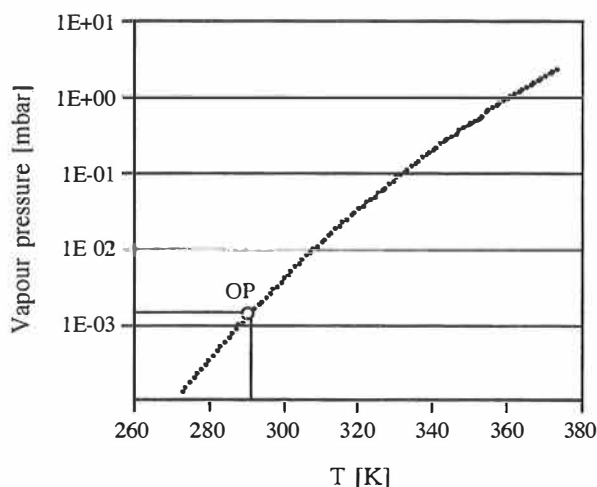


Figure 6.1: Saturated vapour pressure of ferrocene as a function of temperature. The curve has been obtained using the Watson correlation (OP = normal operation point).

6.2. Optimization of the metal ion beam production with the MIVOC method

6.2.1. A brief history and technical arrangement

In the earlier phase of this work, different gaseous compounds were considered for the production of metal ion beams. As a next step, convenient liquids and solid compounds

were studied. Thus, the MIVOC method can be considered as a natural extension of the use of gaseous compounds.

Figure 6.2 shows the original arrangement of the MIVOC system. It was assumed that the evaporation rate of the solid compound is so low and that the saturated vapour pressure is reached slowly. Under these conditions a large quantity of the volatile compound and a large MIVOC chamber would be needed. The large chamber was used as a reservoir of the metal vapour during the ECR run.

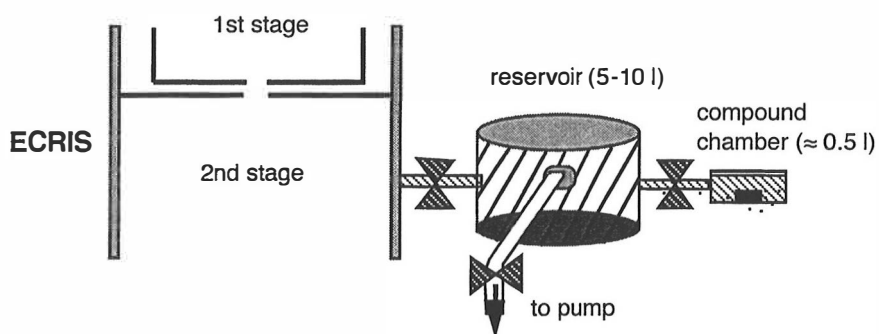


Figure 6.2: A schematic drawing of the original arrangement of the MIVOC-system used with the JYFL-ECRIS.

In addition, the following assumptions were made concerning the advantages of the MIVOC-method:

- a) ECR source is used the same way as for gases (stable, long-term beams)
- b) construction is simple (low cost)
- c) consumption of material is small (rare isotopes can be used)
- d) contamination is minimized or even avoided.

The first advantage leads to a low-cost system. The MIVOC system is durable since no wearing parts are used. The second point follows from the fact that the ion source is used in the same way as with gases. Due to the way the material is fed into the source (diffusion), the ion beam remains stable as long as sufficient material remains in the MIVOC chamber. Items c) and d) will be discussed in the following sections.

For the first MIVOC experiment, the MIVOC chamber was loaded with about 5 g of ferrocene powder ($\text{Fe}(\text{C}_5\text{H}_5)_2$). The chamber was connected to the first stage plasma chamber using a pipe 2 m long with a diameter of 4 mm. Due to the low conductance of

the transmission line, the iron peaks could not be seen in the mass spectrum. A slight heating (up to 60 °C) was also tried but it resulted in contamination of the gas feeding line. However, this contamination of the gas feeding line gave rise to weak iron peaks in the mass spectrum - for example $0.4 \mu\text{A}$ for Fe^{9+} [Koi92].

After accurate conductance calculations, the MIVOC chamber was connected to the second stage plasma chamber using a high conductance transmission line. This resulted in the first successful MIVOC run at room temperature with the ECR ion source. The "test bench" runs using the residual gas analyzer were also started in order to understand the behaviour of the volatile compounds.

6.2.2. MIVOC measurements with the residual gas analyzer

The previously described setup shown in figure 4.1. was used for the study of the compounds of interest. The conductance of the transmission line between the MIVOC chamber and analysis chamber was approximately 0.1 l/s. In all experiments, it was assumed that the ionization efficiency of the analyzer is the same as for air. As a consequence, the results presented may differ by a factor of 2-3 from the absolute values.

6.2.2.a. Optimizing the MIVOC chamber

In a closed volume, the density distribution of molecules is uniform, i.e. the saturation pressure prevails everywhere in the chamber. If the chamber is connected to a pump, the density distribution changes so that the density is lowest at the pump throat. In order to study the dynamics of vaporization at the low pressures involved in the MIVOC method, the effect of the volume of the MIVOC chamber was first investigated.

The ferrocene sample was placed into different size MIVOC chambers. The sample was located close to the pumping port of the chamber. The partial pressure of iron was measured in the analysing chamber of the residual gas analyzer. Results presented in figure 6.3 reveal that the volume of the MIVOC chamber does not affect the partial pressure of ferrocene. This supports the use of a small size chamber (≤ 0.11) because evacuation of moisture from the chamber walls then takes less time.

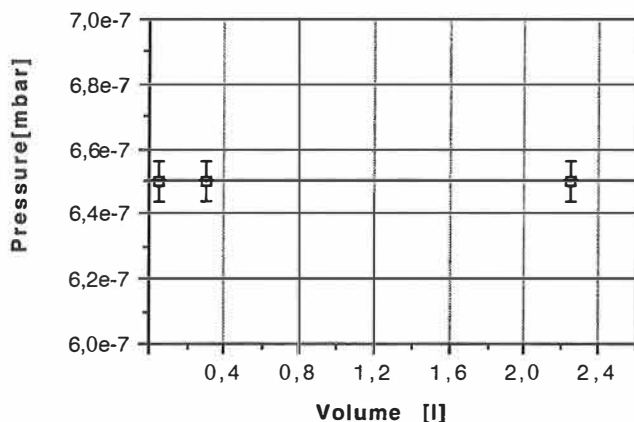


Figure 6.3: Partial pressure of iron in the analysis chamber as a function of the MIVOC chamber volume. About 1 g of ferrocene was placed into the chamber.

6.2.2.b. Determining the minimum sample size and the time to reach vapour saturation

Figure 6.4. shows the vapour pressure of iron inside the analysis chamber of the residual gas analyzer as a function of the mass of ferrocene sample. The graph reveals that the minimum amount of compound which maintains the saturation pressure of ferrocene is

$$m_{min} \approx 3 \text{ mg} \quad (6.5)$$

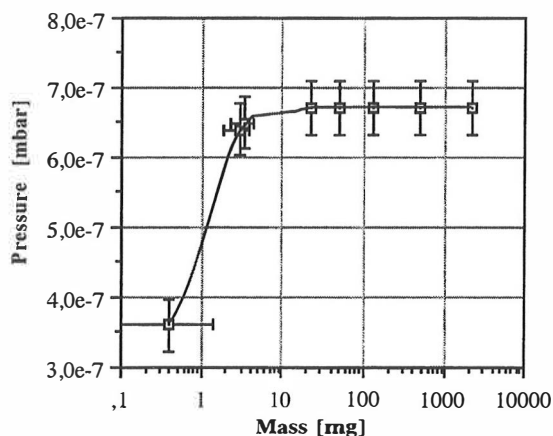


Figure 6.4: Vapour pressure of ferrocene inside the analysis chamber as a function of the mass of the compound.

Under these conditions, the same number of ferrocene molecules are evaporated into the chamber as are evacuated out of the chamber. Increasing the amount of the compound, more than 3 mg in the chamber, does not increase the number of molecules in the chamber volume. On the other hand, a smaller amount will rapidly decrease the number of evaporated molecules. As a result the yield of Fe ions is reduced.

Since the partial pressure of iron in the analysis chamber is $P = 6.5 \times 10^{-7}$ mbar (Fig.6.4) and the pumping speed $S = 75$ l/s, the mass flow rate or throughput of iron is

$$Q_{Fe} = SP = 4.9 \cdot 10^{-5} \text{ mbar l/s} \quad (6.6)$$

The maximum rate for ferrocene evaporation can be estimated as

$$\dot{N}_{Fe, \max} = Q_{Fe} / m_{\min} \approx 1.6 \cdot 10^{-5} \text{ mbar l/s mg}^{-1} \quad (6.7)$$

Evaporation of ferrocene takes place mainly on the powder surface. 3 mg of powder sample covered an area of approximately 3 mm². Actually the ferrocene powder has an uneven and porous surface on the chamber floor which makes the actual evaporating surface much larger. However, for this application it is sufficient to estimate that the optimum, practical surface density for saturation is

$$m_{opt} \approx 1 \text{ mg/mm}^2. \quad (6.8)$$

As a conclusion, an increase in the number of evaporated molecules can take place only through an enlargement of the surface area of the sample. The saturated evaporation pressure remains constant at constant temperature.

In a closed volume, an evaporating compound quickly reaches its saturation pressure. The time required for the saturation is approximately,

$$t_{sat} = P_{sat} V_{MIVOC} / (\dot{N}_{\max} m_{opt}) \quad (6.9)$$

where,

- V_{MIVOC} = volume of MIVOC chamber [l]
- \dot{N}_{\max} = maximum evaporation rate of compound [(mbar l/s)mg⁻¹]
- m_{opt} = mass of compound [mg] at optimum surface density.

When the MIVOC chamber of 0.1 l and 1 g of ferrocene is used, the time of saturation is

$$t_{sat} \approx 10 \text{ ms.} \quad (6.10)$$

6.2.2.c. Average material consumption rate

The material consumption can be measured simply by weighing the sample before and after the ECR ion source run. However, the sample will always contain a small amount of water. In order to investigate the mass loss resulting from the evaporation of water, the residual gas analyzer was used.

The MIVOC chamber, containing about 100 mg of ferrocene powder, was connected to the analysis chamber of the VacScan 100 F measuring setup. The evacuation of the MIVOC chamber was done via a needle valve to avoid the flow of the macroscopic powder particles out of the chamber. After a pumping period of 40 s, the gas analyzer was turned on.

Figure 6.5 shows the ferrocene mass spectra obtained. The left hand picture shows the spectrum measured after two minutes of pumping. Water is the most intense peak indicating that the main mass loss of the measured sample consists of water. The right hand picture shows the spectrum obtained after two hours of pumping. At this time ^{56}Fe was the leading peak so that the main mass losses of the sample consisted of ferrocene. Experience has shown that this condition is required with the JYFL-ECRIS in order to produce highly charged ion beams.

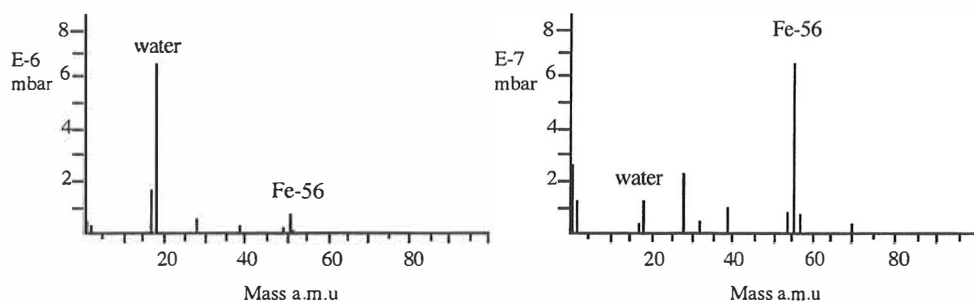


Figure 6.5: The obtained mass spectra of ferrocene after two minutes and after two hours of pumping. The pumping speed in the analysis chamber was about 75 l/s. Note the different pressure scales.

The evaporation of the ferrocene remains constant as long as the amount of the ferrocene sample is at least 3 mg (Section 6.2.2.b). In the MIVOC chamber the

proportion of ferrocene in the residual gas is high compared to water from the walls and the powder. The saturated vapour pressure of water is about four orders of magnitude higher than that of ferrocene. However, the amount of water decreases rapidly when the pumping is started.

Figure 6.6 shows the measured water pressure inside the analysis chamber as a function of time. Fitted curve “P1” correspond to the background pressure of water due to the evaporation from the walls of the MIVOC chamber. Fitted curve “P2” shows the water vapour pressure as a function of time when the crucible containing ferrocene was placed into the MIVOC chamber.

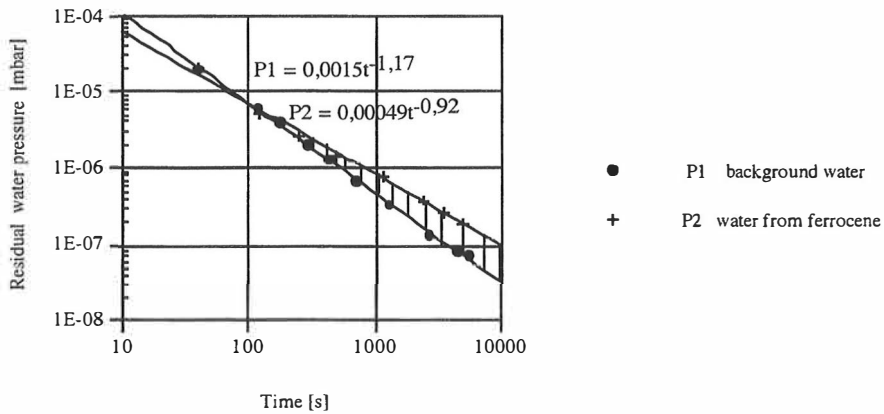


Figure 6.6: Water vapour pressure inside the analysis chamber as a function of the pumping time with and without ferrocene .

During the period of few tens of seconds, the water evaporates mainly from the walls of the chamber and from the surface of the compound. Since water starts to diffuse from the inside of the compound to the surface of the compound, the water pressure decreases more slowly than in the case of the background curve. The mass loss as a result of the evaporation of the water can be determined from the shaded area in figure 6.6.

The pressure of the residual water inside the MIVOC chamber can be expressed as

$$P(t) = At^b \quad (6.11)$$

where A and b are constants and t is time in seconds (Fig. 6.6). The number of molecules in one cubic metre can be solved by using equation (6.12).

$$N = \frac{PV}{kT} \quad (6.12)$$

where P is pressure [Pa], V is volume [m^3], k is the Boltzmann constant and T is the temperature [K]. By combining equations (6.11) and (6.12), the numbers of evacuated molecules during time interval from t_1 to t_2 can be extracted

$$\frac{dN}{dt} = 100 \int_{t_1}^{t_2} \frac{At^b S}{kT} dt \quad (6.13)$$

where the factor of 100 is used to convert mbar to Pa and S is the pumping speed [m^3/s]. The time interval is from the beginning of the shaded area to the end of the measurement. The mass loss in [g] resulting from the evaporation of water from the sample can be estimated using equation (6.14)

$$m = \frac{CM}{(1+b)} \frac{[t_2^{b+1} - t_1^{b+1}]}{N_A} \quad (6.14)$$

where $C = 100AS/kT$, M is the molecule mass in [g/mol] and $N_A =$ Avogadro's constant. The mass loss of the sample during the run of 214 minutes was 7.5 mg. Using equation (6.14) and values in figure 6.6 the mass of evaporated water, $m(\text{P2}) - m(\text{P1})$, was calculated to be 0.1 mg. The amount of the water evaporated before the period of 100 s was also on the order of 0.1 mg. As a conclusion, practically all mass loss was caused by the evaporation of ferrocene.

As the next step, the crucible containing ferrocene powder was placed into the MIVOC chamber. The total weight of the crucible was 1.9070 g before the run. The MIVOC chamber was connected directly to the second stage of the ECR ion source and it was carefully evacuated through the accurate leak valve during 10 minutes. After the run of 16.1 hours, the crucible was weighed at 1.8910 g. This corresponds to a consumption rate of 0.99 mg/h.

The material consumption rate in the case of ferrocene was defined to be about 1 mg/h, i.e.

$$Q_{\text{Fe}} \approx 0.3 \text{ mg/h} \quad (6.15)$$

for pure iron. This corresponds to $0.12 \text{ cm}^3/\text{h}$ (NTP) of vapour. In the above mentioned experiment, the ion beam intensity was maximized for Fe^{11+} . In section 5.13, it was shown that the material consumption rate decreased as a function of the charge state, i.e. for charge states higher than $q=11$, consumption rates less than 0.3 mg/h can be achieved. This result demonstrates, that the consumption rate of material with the MIVOC method is very low.

6.2.3. Carbon contamination

The MIVOC compound always contains one or more unwanted elements, usually carbon and hydrogen which are extra, useless and sometimes harmful elements for the beam production. In the ECR plasma, the compound decomposes into its constituent elements. Figure 6.7 shows the iron mass spectrum measured with the RIKEN 18 GHz ECR ion source using the MIVOC method [Nak97]. During this experiment no mixing gas was used. As can be seen, the spectrum is dominated by iron. With the aid of figure 6.7, the total iron ion beam was estimated to be about $39 \mu\text{A}$. The total carbon current from the spectrum was estimated to be $64 \mu\text{A}$, i.e. iron ionization efficiency is 6 times higher than that of carbon ($\text{Fe}(\text{C}_5\text{H}_5)_2$). Another spectrum measured for ferrocene gives a value of 3 times higher. In this case the carbon ions were the leading peaks in the spectrum. The studies and experience with ferrocene indicates, that the ionization efficiency of iron is higher than that of carbon. However, in these cases the ECRIS was optimized for the production of iron beams. Different results might be obtained when the ion source is tuned and optimized for carbon. The low ionization efficiency of carbon is supported by the studies in the sections 3.1.2 and 5.1.4 i.e. which indicates carbon to be weakly confined in the iron plasma.

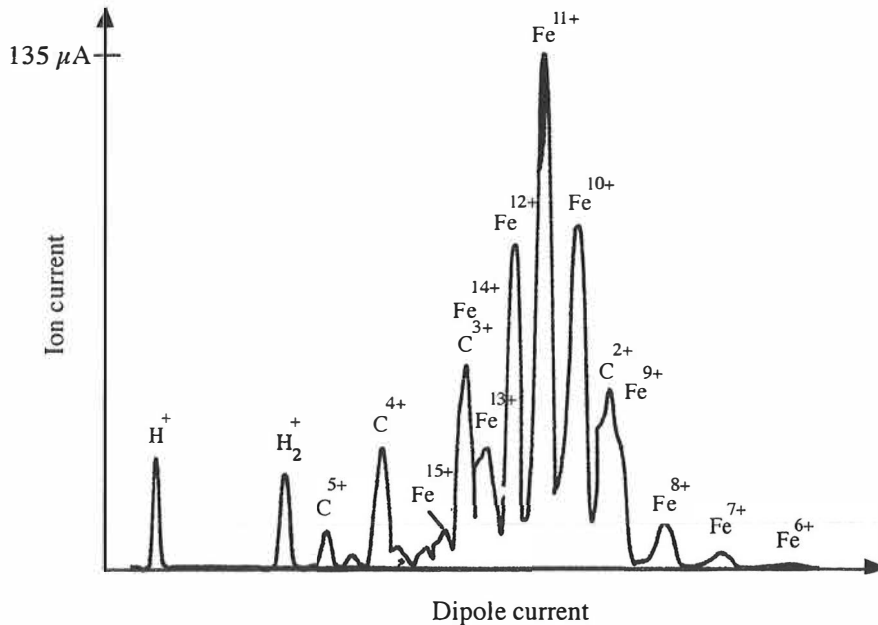


Figure 6.7: The iron ion beam intensity as a function of the analyzing magnet current. The maximum intensity of Fe^{11+} ion beam was $135 \mu\text{A}$ using ferrocene compound with the RIKEN 18 GHz ECRIS without gas mixing. Extraction voltage was 10 kV [Nak97].

The question of the contamination was also studied simply by means of mass spectra obtained before and after the MIVOC runs. No trace of the metal ion beams (for example iron or nickel) has been noticed in subsequent ECRIS runs. However, the plasma chamber walls were contaminated by carbon. This is likely to decrease the secondary electron emission yield from the walls of the plasma chamber. Consequently, carbon contamination is considered to be the most serious drawback of the MIVOC method. To minimize the consequences of this effect, the plasma chamber is lined with a removable aluminum foil.

6.2.4. Summary of the development work

The measurements with the ferrocene compound showed that only a small amount of the compound is needed to maintain the saturated vapour pressure inside the MIVOC chamber during the ECRIS run. This minimum sample size is less than 10 mg. The material consumption rate is on the order of 1 mg/h of compound when gas mixing is used. It is reasonable to use a sample size related to the consumption of the material during the run. For example, for a run of 5 days approximately 120 mg of compound is needed. The saturated vapour pressure inside the MIVOC chamber is reached within tens of milliseconds. This requires that the minimum sample size is exceeded and the powder is scattered widely on the bottom of the MIVOC chamber.

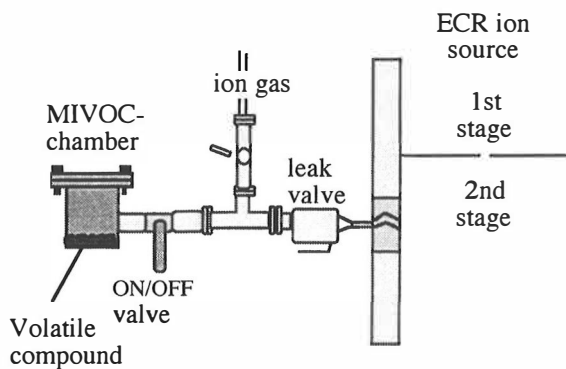


Figure 6.8: A schematic picture of the MIVOC chamber connected to the ECR ion source.

Figure 6.8 shows the present MIVOC system based on the research and development work reported here. No reservoir is needed and a MIVOC chamber of a small volume (less than 0.1 litre) is used to minimize the amount of water contamination. The chamber is located as near to the ECR ion source as possible to maximize the conductance of the transmission line. In addition, a large aperture transmission line is

used in order to increase the throughput. The vapour is allowed to diffuse into the plasma where the molecules are decomposed and ionized by the hot electrons. As simple a compound as possible should be used to optimize the production of the metal ion beams. In addition the desired element has to be the heaviest element in the compound. This way the feed rate of the neutrals and contamination of the ion source are also minimized.

7. Metal ion beams produced with the MIVOC method

Most of the MIVOC beams have been produced using metallocene compounds. The atom between the cyclopentadiene rings can be replaced at least by Mg, Co, Mn and Os. Most of the metallocenes are classified as easily handled but harmful chemical compounds. However, magnesocene is spontaneously flammable in air. Table 7.1 shows the structure and properties of ferrocene and nickelocene.

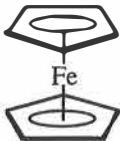
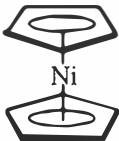
	<u>Ferrocene</u> $\text{Fe}(\text{C}_5\text{H}_5)_2$	<u>Nickelocene</u> $\text{Ni}(\text{C}_5\text{H}_5)_2$
		
Molecular weight	186.04 g	188.90 g
Melting point	174-176 °C	171-173 °C
Boiling point	249 °C	sublimes at 130 °C
Vapour pressure (20 °C)	1.7x10 ⁻³ mbar	3.5x10 ⁻³ mbar

Table 7.1: Chemical structures and physical properties of ferrocene and nickelocene.

Another useful group is carbonyls of metals such as Fe, Ni, Co, Cr and Mo. However, most of the carbonyls are extremely toxic, especially $\text{Ni}(\text{CO})_4$. Their toxic nature must be considered before they are used as MIVOC compounds. Naturally, all chemical compounds must be handled according to the recommendations.

7.1. The Mg ion beam

Magnesium is a strongly electropositive metal and its existing metal-organic compounds tend to have a very low vapour pressure. In addition, many of them decompose spontaneously at room temperature conditions. Magnesium has three stable isotopes with abundances of 78.99 %, 10.00 % and 11.01 % for $^{24,25,26}\text{Mg}$, respectively. A magnesium ion beam can be produced by using magnesocene, $\text{Mg}(\text{C}_5\text{H}_5)_2$. The compound is moisture sensitive and tends to ignite spontaneously in the air. Thus, special care has to be taken in handling it.

The Mg mass spectrum obtained with the residual gas analyzer is shown in figure 7.1. The partial pressures of the isotopes $^{24,25,26}\text{Mg}$ were found to be $2.7 \cdot 10^{-6}$ mbar,

$4.1 \cdot 10^{-7}$ mbar, and $4.9 \cdot 10^{-7}$ mbar, respectively. The isotopic abundances calculated from these values are 75%, 11.4 % and 13.6 %, respectively. The close agreement of the measured abundances with the known values indicates that the observed peaks are due to Mg ions rather than their chemical compounds.

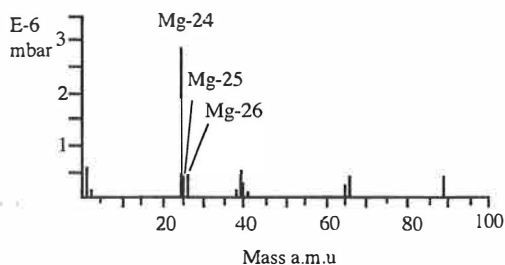


Figure 7.1: Magnesocene mass spectrum measured with the residual gas analyzer.

The MIVOC chamber with a volume of about 0.1 l, charged with magnesocene, was connected to the second stage of the ECR ion source. The ECRIS was operated with nitrogen as the mixing gas. The best gas mixing ratio turned out to be about 5-10 % of magnesocene vapour in nitrogen. A brief optimization run yielded the following values of the main source parameters: Total microwave power 135 W, of which 20 % was fed into the first stage and 80 % into the second stage. The plasma-on pressure in the first stage was $3.9 \cdot 10^{-6}$ mbar and in the second stage $4.0 \cdot 10^{-7}$ mbar. The plasma cathode voltage was used to maximize the ion current.

The ion beam spectrum obtained is shown in figure 7.2. The beam was tuned for $^{24}\text{Mg}^{5+}$ and all Mg^{q+} intensities were subsequently measured. The corresponding ion currents observed for the various charge states of the Mg isotopes are shown in table 7.2. A further tuning of $^{24}\text{Mg}^{5+}$ resulted in an ion current of $11.8 \mu\text{A}$. No magnesium contamination was observed in a subsequent $^{36}\text{Ar}^{8+}$ run.

q	3+	4+	5+	6+	7+	compound $\text{Mg}(\text{C}_5\text{H}_5)_2$
^{24}Mg	5.3	* 10.1	9.8	† 7.2	‡ 1.8	
^{25}Mg	0.65	1.2	1.2	1.0	* 0.23	
^{26}Mg	0.67	1.4	1.3	1.0	0.25	

Table 7.2: Currents in μA from magnesocene with a natural composition of Mg (^{24}Mg 78.99%, ^{25}Mg 10.00% and ^{26}Mg 11.01%). Asterisks denote cases where the value was calculated from the ^{26}Mg isotope of the same charge state.

The even charge states of ^{24}Mg ions are overlapped by ^{12}C . The ion currents of $^{24}\text{Mg}^{4+,6+,7+}$ have been calculated from the measured currents of $^{26}\text{Mg}^{q+}$ isotopes at the same charge states using the known isotopic abundance. The procedure is justified because the magnesium is separated from carbon or residual oxygen in the K130 cyclotron. The residual oxygen contamination in the $^{24}\text{Mg}^{3+}$ peak is less than 5%. During the one week magnesium run, the ion beam was very stable without any further tuning of the ECR ion source required. The intensity of the Mg^{5+} ion beam was $0.5 \mu\text{A}$ on the experimental target (after the K130 cyclotron).

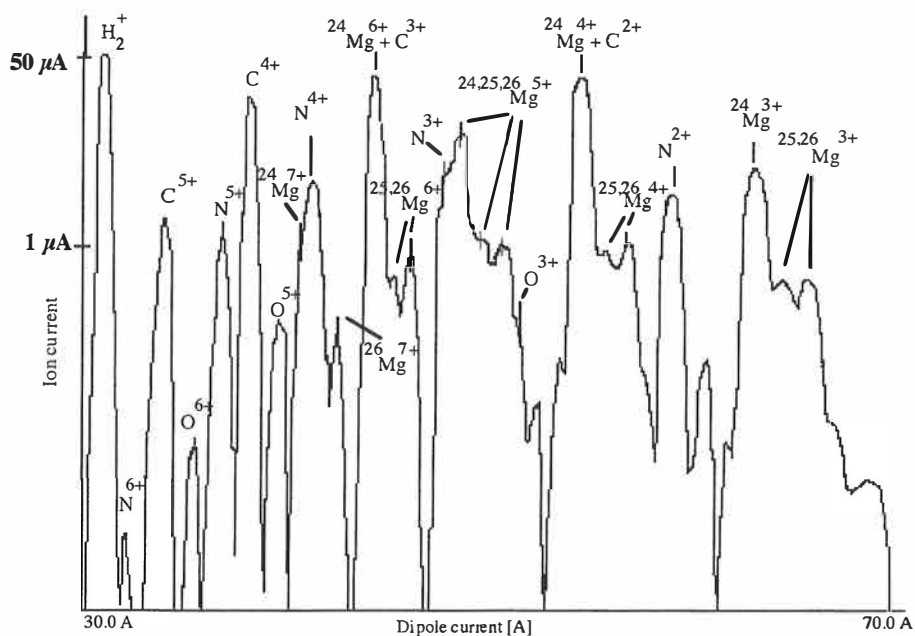


Figure 7.2: Mg spectrum from magnesocene powder $\text{Mg}(\text{C}_5\text{H}_5)_2$ at room temperature using the MIVOC method with the JYFL-ECRIS. Nitrogen was used as a mixing gas. The intensity scale is logarithmic.

7.2. The Si ion beam

The silicon beam has normally been produced using silane, SiH_4 , which is in a gaseous state at room temperature. At the Accelerator Laboratory, the silicon beam has been produced using the MIVOC method in order to make the production of metal beam cocktails and $^{29,30}\text{Si}$ ion beams feasible.

Two different compounds have been tested. Figure 7.3 shows the mass spectrum of tetramethylsilane, $\text{Si}(\text{CH}_3)_4$, measured with the residual gas analyzer. The masses of the

isotopes of $^{28,29,30}\text{Si}$ were not found in the spectrum which indicates that the compound was not decomposed by the filament of the analyzer or the pressure of the compound was smaller than assumed. However, the peaks at masses 73, 74 and 75 are probably from the compound with one CH_3 -group missing. The isotopic abundancies calculated from the spectrum are 89.7% (92.23%), 7.1% (4.67%) and 3.6% (3.10%) with the known abundances shown in parenthesis. The close agreement between the measured and known values indicates that $^{28,29,30}\text{Si}(\text{CH}_3)_3$ molecules are formed in the breakup of the tetramethylsilane. A similar spectrum was obtained using tetrakis(trimethyl)silylsilane ($\text{Si}[\text{Si}(\text{CH}_3)_3]_4$). This compound is solid at room temperature. Tetramethylsilane is liquid.

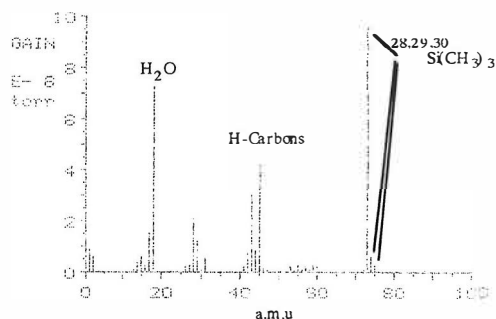


Figure 7.3: The mass spectrum of tetramethylsilane measured with the residual gas analyzer.

Both compounds were tested in the ECR ion source. During the one day test the ion source was tuned for the Si^{5+} beam. Oxygen was used as a mixing gas. The maximum current of

$$\text{Si}^{5+} \text{ was } 6 \text{ and } 10 \mu\text{A}$$

when tetrakis(trimethyl)silylsilane and tetramethylsilane were used as a MIVOC compounds, respectively. As a comparison, the normal intensity of Si^{5+} ion beam is of the order of $15 \mu\text{A}$ when silane is used.

7.3. The Fe and Ni ion beams

Figure 7.4 shows spectra of ferrocene and nickelocene measured by the residual gas analyzer. The spectra show ^{56}Fe and ^{58}Ni as the leading masses. As typical residual gases, water vapour and nitrogen appear in the spectrum. Also Fe isotopes 54 and 57

and Ni isotope 60 are present. When the connecting needle valve was closed, the metal peaks disappeared in a few seconds, indicating that no noticeable contamination occurred.

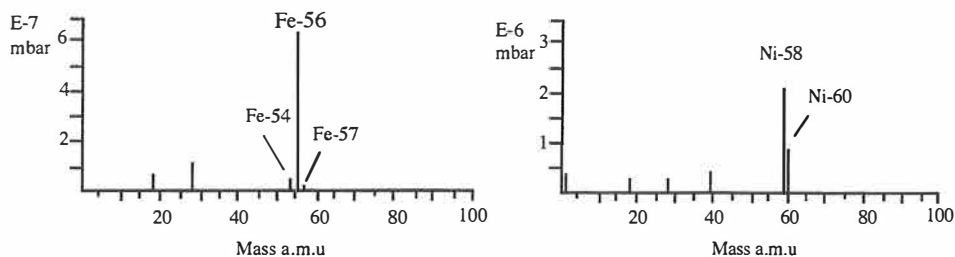


Figure 7.4: Ferrocene and nickelocene mass spectra with the residual gas analyzer. Note the different pressure scales.

For the production of high charge states, nitrogen was more effective than helium as a mixing gas. The best gas-mixing ratio was found to be 5-10 % of ferrocene/nickelocene vapour with nitrogen. The highest intensities of highly charged ions were produced with total microwave power of about 160 W. Power was divided between the two stages, 20 % into the first stage and 80 % into the second stage. The optimum plasma cathode voltage was -55 V and the distance between the two plasma stages was 9 mm. Table 7.3 shows the best results presently achieved using the MIVOC method with iron and nickel compounds in the JYFL-ECRIS. An iron spectrum measured with the RIKEN 18 GHz ECRIS is shown in figure 6.7 [Nak97].

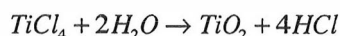
q	9+	10+	11+	12+	13+	14+	15+	Compound
^{56}Fe	23.9	23.4	17.6	*	5.9	*	1.1	$\text{Fe}(\text{C}_5\text{H}_5)_2$
^{58}Ni	14.1	18.7	*	8.8	5.6	2.6	1.2	$\text{Ni}(\text{C}_5\text{H}_5)_2$

Table 7.3: Currents in μA from elements of natural composition of elements, having abundances of ^{56}Fe 92 % and ^{58}Ni 68 %. Asterisks denote when overlapped with other ions.

7.4. MIVOC beams of Ti, Cr, Co, Cu and Ge

The vapour pressure of titanium is quite low making the use of a conventional oven impossible. With the JYFL-ECRIS a titanium beam has been produced using the

MIVOC method using titanium(IV)chloride, $TiCl_4$ [Koi97a]. This compound is rather difficult to use. It reacts violently with water as follows:



The vapour pressure of HCl is very high compared to $TiCl_4$. As a result, a very strong chlorine peak was noticed in the mass spectrum instead of titanium. Since large amounts of HCl can be very harmful to the ion source and the vacuum system, a small amount of CaO was mixed with $TiCl_4$. As a result, the intensity of Ti compared to HCl^+ in the mass spectrum measured by the residual gas analyzer increased.

The left hand spectrum in figure 7.5 corresponds to the normal residual mass spectrum in the early phase of the development work. The right hand spectrum was measured when special attention was paid to storage and handling of the compound. The maximum intensity of the Ti^{10+} beam, measured after the cyclotron, was $0.2 \mu A$. The major drawback when using this compound is a substantial chlorine contamination of the ECR ion source. For several days after the titanium run, a chlorine beam was observed.

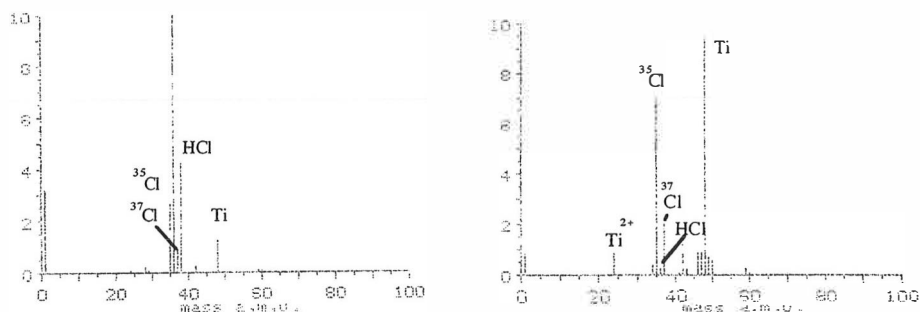


Figure 7.5: Two Titanium(IV)chloride mass spectra measured under different conditions with the residual gas analyzer.

A chromium ion beam was produced using chromiumhexacarbonyl ($Cr(CO)_6$). The maximum current of Cr^{12+} beam was measured to be $2.6 \mu A$. A cobalt ion beam can be produced using cobaltocene ($Co(C_5H_5)_2$) or di-cobalt octacarbonyl ($Co_2(CO)_8$). The maximum current of the Co^{12+} beam was $1.5 \mu A$ using the carbonyl compound. A copper ion beam was produced from copper(II)hexafluoroacetylacetonate hydrate ($[CF_3COCH=C(O)CF_3]_2Cu \cdot xH_2O$). During a test period of two days, the beam intensity of $^{63}Cu^{11+}$ was only $0.5 \mu A$. A germanium ion beam was obtained using

tetraethylgermanium ($\text{Ge}(\text{CH}_2\text{CH}_3)_4$). The on-target intensity (after the K130 cyclotron) of Ge^{13+} was about $0.1 \mu\text{A}$. Table 7.4 shows the intensities of different elements.

q	10+	11+	12+	13+	Compound
Ti	0.2*				TiCl_4
Cr			2.6		$\text{Cr}(\text{CO})_6$
Co			1.5		$\text{Co}_2(\text{CO})_8$
Cu		0.5			See table 7.5
Ge				0.15*	$(\text{Ge}(\text{CH}_2\text{CH}_3)_4)$

Table 7.4: Intensities of different metal ion beams in μA . Asterisk denoted when current measured after the cyclotron.

7.5. Ion beams from rare isotopes

Due to the low material consumption with the MIVOC method, expensive isotopes can be used in an economical way. Ferrocene and nickelocene with natural iron and nickel replaced by the rare isotopes, ^{54}Fe and ^{60}Ni , were synthesized at the Department of Chemistry, University of Jyväskylä. The behaviour of these compounds in the residual gas analyzer was similar to the normal ferrocene and nickelocene already used with the JYFL-ECR ion source. Figure 7.6 shows the nickelocene mass spectra with the residual gas analyzer.

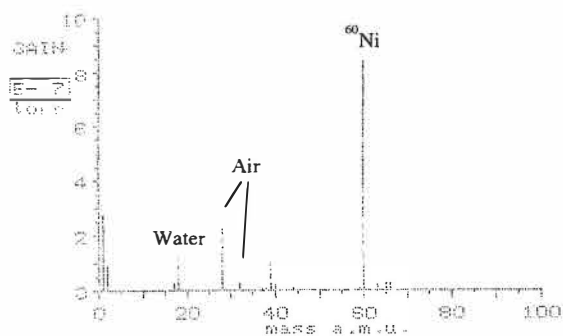


Figure 7.6: The mass spectrum of the ^{60}Ni from a synthesized nickelocene with the residual gas analyzer.

The first isotope run with the K130-cyclotron was carried out using ferrocene in order to produce a 275 MeV ^{54}Fe beam. The ECR ion source was tuned for Fe^{11+} and nitrogen was used as a mixing gas. During the run of 120 hours, the ferrocene consumption was

179 mg, i.e. 0.43 mg/h of iron. This value is slightly higher than expected compared to the material consumption rate of other MIVOC beams.

Figure 7.7 shows the mass spectrum of ^{54}Fe . The consumption rate of iron corresponds to $0.18 \text{ cm}^3/\text{h}$. At the same time, the consumption rate of nitrogen was $1.4 \text{ cm}^3/\text{h}$. The iron charge state distribution was peaked towards $^{54}\text{Fe}^{8+}$, which indicates that the ferrocene mixing ratio was too high. This is a probable explanation for the relatively high consumption rate.

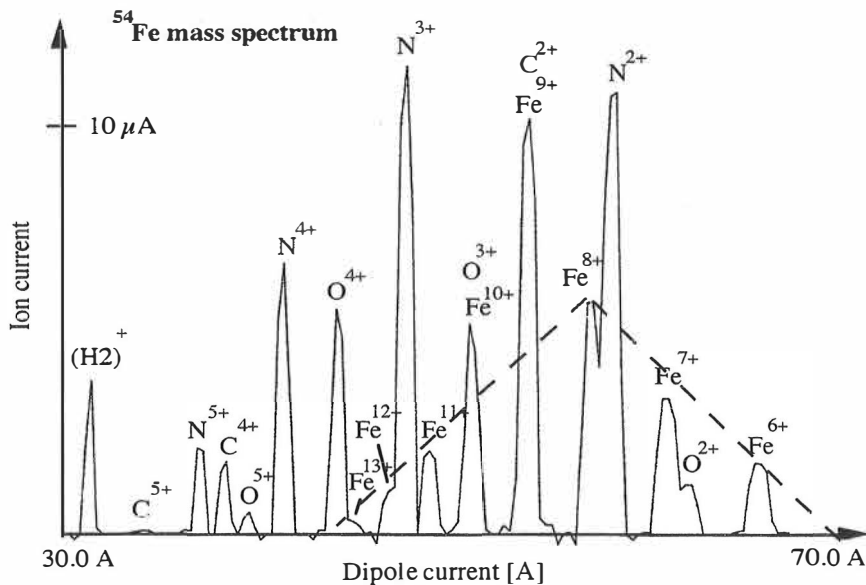


Figure 7.7: ^{54}Fe spectrum from the synthesized ferrocene powder $^{54}\text{Fe}(\text{C}_5\text{H}_5)_2$ at room temperature using the MIVOC method with the JYFL-ECR ion source. The dashed line shows approximately the charge state distribution of iron.

7.6. Cocktail beams

“Beam cocktails” are used when several ion beams are needed during a single experiment. Ions with nearly the same q/A ratio are needed in order to inject different ion beams into the cyclotron at the same time. Most of the ions with approximately the same q/A ratio can be resolved inside the cyclotron. Different beams can be extracted quickly by changing the magnetic field of the cyclotron.

The q/A ratio of $^{16}\text{O}^{2+}$, $^{24}\text{Mg}^{3+}$, $^{40}\text{Ar}^{5+}$ and $^{56}\text{Fe}^{7+}$ is 0.125. They cannot be resolved using the normal analyzing magnet. As a consequence, the ions are fed into the cyclotron at the same time. However, accurate mass calculations show that the smallest

q/A difference of 0.2 ‰ is between the argon and iron indicating that the above mentioned elements can be resolved inside the cyclotron.

In the case of the first beam cocktail, the oxygen and argon were mixed into the mixing gas feed line. The mixing ratio was about 30 % of argon in oxygen. The magnesium and iron ion beams were produced using the MIVOC method. Magnesocene and ferrocene compounds were both mixed into the MIVOC chamber which was directly connected to the second stage of the ECR ion source. A few hundreds of milligrams of BaO was mixed with the magnesocene and ferrocene for drying.

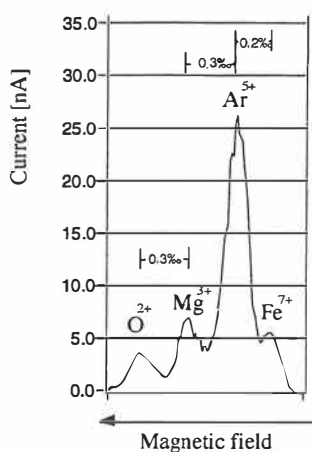


Figure 7.8: Mass spectrum measured after the cyclotron. Ions shown in the spectrum were injected in the cyclotron at the same time. They were extracted by slightly changing the magnetic field of the cyclotron.

Figure 7.8 shows the mass spectrum obtained after the cyclotron. The magnetic field was scanned by changing the current of the outermost trim coil. The accurate values of the q/m differences are presented in the mass spectrum.

7.7. MIVOC compounds used with the JYFL-ECRIS

Ferrocene was the first MIVOC compound successfully used to produce a metal ion beam. Its vapour pressure measured with the residual gas analyzer was used as a reference when other MIVOC compounds were sought. A new compound was tested in the ECR ion source if the value of P_n/P_r was approximately 1 or higher (P_n denotes the vapour pressure of new compound and P_r the vapour pressure of ferrocene).

Table 7.5. shows compounds that have been used with the JYFL-ECRIS. As simple a compound as possible has to be found in order to maximize the beam intensity and to

minimize the contamination of the ion source. For example, a possible explanation for the low intensity of the copper ion beam can be the result of the large amount of other components in the compound.

Element	Compound	P_n/P_f
Mg	$Mg(C_5H_5)_2$	4.3
Si	$Si(CH_3)_4$	>15
Ti	$TiCl_4$	>15
Cr	$Cr(CO)_6$	>1.5
Fe	$Fe(C_5H_5)_2$	1
Co	$Co_2(CO)_8$	*
Ni	$Ni(C_5H_5)_2$	3.1
Cu	$[CF_3COCH = C(O-)CF_3]_2Cu \cdot xH_2O$	1.5
Ge	$(Ge(CH_2CH_3)_4)$	>15

Table 7.5: The MIVOC compounds that have been used for the production of metal ion beams with JYFL-ECRIS. Here P_n = vapour pressure of new compound, P_f = vapour pressure of ferrocene. Pressures were measured with the residual gas analyzer. Asterisks denote when value has not been measured.

8. Summary and discussion

The goal of this work was to make metal ion beams available at the Accelerator Laboratory, University of Jyväskylä. Using the MIVOC technique, developed in this work, a number of metal ion beams were produced with the JYFL-ECR ion source. Solid or liquid compounds of metals that have a room temperature vapour pressure on the order of 1×10^{-3} mbar or higher were used.

As a first step the literature was searched for compounds fulfilling the MIVOC pressure requirement. Due to the lack of information on vapour pressures of the compounds, the vapour pressures were in some cases estimated from thermodynamic data. The most promising candidates were then tested with the residual gas analyzer. A sample of the volatile compound was placed in a small vacuum chamber connected to the analyzer. After a successful analyzer test, the same chamber was connected to the ECR ion source. The vapour was then allowed to diffuse into the plasma chamber as an ion gas. There the components of the vapour were ionized and extracted as highly charged ion beams.

Parallel to the above described activity, the tuning of the ECR ion source was extensively studied in order to maximize the intensity of the metal ion beams. The electron density inside the plasma can be enhanced using several techniques in order to increase the intensity of highly charged ions. In this work it was noted that the aluminum foil liner in the second stage chamber and a negative voltage applied to the first stage of the source were efficient methods for enhancing the electron density in the plasma. However, carbon contamination from the MIVOC compounds on the aluminum foil decreases the yield of secondary electrons. This problem is avoided in the case of the plasma cathode method. In addition, the electron density can be adjusted by changing the negative voltage of the plasma cathode. No additional improvements are noted when both methods were used simultaneously.

The ECR ion source must be carefully tuned when highly charged metal ion beams are required. Any changes inside the ion source strongly affect the ion current of the metal beams. Consequently a new, highly stabilized gas feeding system was developed to maintain a constant pressure inside the ion source. The new system has significantly decreased the need of tuning the ion source during runs.

In the comparison of the metal ion beam performance of the JYFL-ECRIS equipped with the MIVOC system with other ECR ion sources using other metal beam techniques, the overall performance of the sources needs to be taken into account. The JYFL-ECRIS was designed and constructed more than 10 years ago and since that time many new techniques have been incorporated in newer ECR ion sources. In spite of this, intensities of metal ion beams from the JYFL-ECRIS are comparable to those achieved with other sources. At RIKEN in Japan, the MIVOC technique has been adopted for use with one of the most advanced ECR ion sources presently available, the RIKEN 18 GHz ECRIS. With the MIVOC technique, experiments at RIKEN resulted in some of the highest ion beam intensities for many metal elements [Nak97].

The MIVOC method has proved to be both reliable and simple in routine operation. For example, during a two-week nickel run no adjustment of the ECR ion source was required. In addition, the method is very time efficient since no ventilation or pump-down of the ion source is needed in changing between different metal ion beams. The construction is simple since the MIVOC chamber is used like a simple gas cylinder. The only difference, compared to a normal gas bottle, is that the gas pressure inside the MIVOC "bottle" is very low - on the order of 10^{-3} mbar. Measurements have also shown that the material consumption rate is quite reasonable, i.e. less than 1 mg/h. Consequently the four advantages of this method assumed earlier (easy to use, simple construction, small consumption of material, minimal contamination) are well fulfilled, except for the carbon contamination of the source. This drawback, however, is minimized by using a removable Al-foil in the second stage of the source.

The MIVOC method has been adopted at several laboratories [Wal95, Nak96, Yok95, Bex97, Kit97, Ull97,]. Presently, at least 17 different beams have been produced (C, Mg, Si, Cl, Ti, V, Cr, Fe, Co, Ni, Ge, Mo, Ru, Sn, I, W and Os) by using this method (see figure 8.1).

H 1																	He 2
Li 3	Be 4											B 5	C 6	N 7	O 8	F 9	Ne 10
Na 11	Mg 12											Al 13	Si 14	P 15	S 16	Cl 17	Ar 18
K 19	Ca 20	Sc 21	Ti 22	V 23	Cr 24	Mn 25	Fe 26	Co 27	Ni 28	Cu 29	Zn 30	Ga 31	Ge 32	As 33	Se 34	Br 35	Kr 36
Rb 37	Sr 38	Y 39	Zr 40	Nb 41	Mo 42	Tc 43	Ru 44	Rh 45	Pd 46	Ag 47	Cd 48	In 49	Sn 50	Sb 51	Te 52	I 53	Xe 54
Cs 55	Ba 56	La 57	Hf 72	Ta 73	W 74	Re 75	Os 76	Ir 77	Pt 78	Au 79	Hg 80	Tl 81	Pb 82	Bi 83	Po 84	At 85	Rn 86
Fr 87	Ra 88	Ac 89															
		103	104	105	106	107											

Figure 8.1: Black triangles denote the elements that are available using the MIVOC method.

Most ion beams lighter than krypton have now been produced with the JYFL-ECR ion source. Future requirements are likely to lead to the development of beams from heavier species.

Near future plans include the application of the MIVOC method to compounds having room temperature vapour pressure lower than 10^{-5} mbar by using a unheated miniature oven as a MIVOC chamber. This technique can be expected to expand the selection of metal ions available.

References:

- [Ant86] T.A.Antaya and Z.Q.Xie, Proc. of the 7th Int. Workshop on ECR Ion Sources, Jüli-Conf-57, ISSN 0344-5798, KFA Jülich GmbH, (1986), p. 72.
- [Ant89] T.A. Antaya, Proc. of the Int. Conference on ECRIS, Grenoble, 1988, p.C1-707.
- [Ant94] T.A.Antaya and S. Gammino, Rev. Sci. Instrum, 65 (5), May, (1994), p. 1723.
- [Ard65] W.B.Ard, R.A.Dandl, A.C.England, G.M. Haas and N.H. Lazar, Proc. Conf. on Plasma Physics and Controlled nuclear fusion research, Culham, 1965, Vol. II, p. 153.
- [Ari81] J.Arianer and R.Geller, Annu. Rev. Nucl. Part. Sci. Vol.31, (1981), p. 19.
- [Ber58] I.B.Bernstein, Phys. Rev., Vol 109, Number 1, Jan., (1958), p. 10.
- [Ber72] K.Bernhardi and K.Wiesemann, Plasma Phys. 14, (1972), p. 1073.
- [Beu85] H.Beuscher, Proceedings of the 6th Workshop on ECR Ion Sources, Berkeley, 1985, p. 107.
- [Bex97] L.Bex, J.L.Flambard, M.Dupuis, P.Lehérisier, and J.P.Rataud, Contributed paper to ICIS97
- [Bir95] S.Biri, A.Valek and J.Vámosi, Proc. of the 12th Int. Workshop on ECR Ion Sources, April 25-27, RIKEN, Japan, (1995), p. 207.
- [Bli72] S.Bliman, R.Geller, W. Hess and B.Jacquot, IEEE Trans. Nucl. Sci. NS-19, (1972), p. 200.
- [Bou82] F.Bourg, R.Geller, B.Jacquot, M.Pontonier, Proc. of the 4th Int. Workshop on ECRIS, Grenoble, 1982, edited by M. C. Boraso, CENG, p. 5.1.
- [Che74] Francis F.Chen, Introduction to plasma physics, ISBN 0-306-30755-3, Plenum press, (1974).
- [Cla88] D.J.Clark and C.M.Lyneis, Proceedings of the International Conference on ECRIS, Grenoble, 1988, p. C1-759.
- [CRC77] Handbook of chemistry and physics, 58th edition 1977-1978, CRC press.
- [Del92] M.Delaunay, Review of the Scientific Instrumentation, 63, 1992, p. 2861.
- [Dre85] A.G.Drentje, Proc. of the 6th Workshop on ECR Ion Sources, Berkeley, 1985, p.73.
- [Dre92] A.G.Drentje, Review of the Scientific Instrumentation, 63, 1992, p. 2875.

- [Dre93] A.G.Drentje, Proceedings of the 11th International Workshop on Electron Cyclotron Resonance Ion Sources, May 6-7, Groningen, (1993), p. 155.
- [Eng83] A. von Engel, Electric plasmas: their nature and uses, ISBN 0-85066-147-1, Taylor & Francis Ltd, London and New York, (1983)
- [Fon86] A.Fontell, J.Maula, R.Nieminen, C.Söderlund, K.Valli, A.Vehanen, M.Vulli and M.Ylilammi, Tyhjiötekniikka, ISBN 951-794-422-5 (1986).
- [Fri93] L.Friedrich, E.Huttel, R.Hentschel and H.Tyroff, Proceedings of the 11th International Workshop on Electron Cyclotron Resonance Ion Sources, May 6-7, Groningen, (1993), p. 19.
- [Gam92] S.Gammino, J.Sijbring and A.G.Drentje, Rev. Sci. Instrum., 63(4), April (1992), p. 2872.
- [Gel83] R.Geller and B.Jacquot, Phys. Scripta T3, (1983), p.19.
- [Gel86] R.Geller and B.Jacquot, Contributed Papers of the 7th Workshop on ECR Ions Sources, ISSN 0344-5798, 1986, p. 31.
- [Gel87] R.Geller, F.Bourg, P.Briand, J.Debernardi, M.Delaunay, B.Jacquot, P.Ludwig, R.Pauthenet, M.Pontonnier and P.Sortais, Proc. of the 11th Int. Conf. on Cyclotrons and their Applications, Tokyo, 1987, p.1
- [Gel90] R.Geller, Ann. Rev. Nucl. Part. Sci. Vol.40, (1990), p. 15.
- [Gel92] R. Geller, P.Ludwig and G.Melin, Review of Scientific Instruments, Proceeding of the 4th International Conference on Ion Sources, Vol. 63, (1992), p. 2795.
- [Gel93] R.Geller, Proceedings of the 11th International Workshop on Electron Cyclotron Resonance Ion Sources, May 6-7, Groningen, (1993), p. 1.
- [Gel96] R.Geller, Electron Cyclotron Resonance Ion Sources and ECR Plasmas, Published by Institute of Physics Publishing, (1996), ISBN 0 7403 0107 4.
- [Gol90] K.S.Golovanivsky and G.Melin, Proc. of the 10th Int. Workshop on ECR Ion Sources, CONF-9011136, ORNL, Nov. 1-2, (1990), p. 63.
- [Gol93] K.S. Golovanivsky, Proceedings of the 11th International Workshop on Electron Cyclotron Resonance Ion Sources, May 6-7, Groningen, (1993), p. 78.
- [Gol95] K.S. Golovanivsky, Proc. of the 12th Int. Workshop on ECR Ion Sources, April 25-27, RIKEN, Japan, (1995), p. 329.
- [Gold95] R.J Goldston and P.H. Rutherford, Introduction to plasma physics, ISBN 0-7503-0325-5, Institute of Physics Publishing, Bristol and Philadelphia, (1995).
- [Har94] R. Harkewicz, J. Stacy, J. Greene and R.C. Pardo, Review of the Scientific Instrumentation, 65, 1994, p. 1104.

- [Har95] R.Harkewicz, P.J.Billquist, J.P.Greene, J.A.Nolen, Jr. and R.C. Pardo, *Rev. Sci. Instrum.* 66 (4), April (1995), p. 2883.
- [Har96] R. Harkewicz, *Rev. Sci. Instrum.* 67 (6), June (1996), p. 2176.
- [Hav89] C.C.Havener, M.S.Huq, F.W.Meyer and R.A.Phaneuf, *Colloque de Physique, Colloque No1, Suppl. J. de Physique, FASC.1(1989)*, p. C1-7.
- [Hit93] D.Hitz, G.Melin, M.Pontonnier and T.K.NGuyen, *Proc. of the 11th Int. Workshop on Electron Cyclotron Resonance Ion Sources*, May 6-7, Groningen, (1993), p. 91.
- [Hit95] D.Hitz, F.Bourg, P.Ludwig, G.Melin, M.Pontonnier and T.K.NGuyen, *Proc. of the 12th Int. Workshop on ECR Ion Sources*, April 25-27, RIKEN, Japan, (1995), p. 126.
- [Jac90] B.Jacquot and M.Pontonnier, *Nucl. Instr. and Meth. in Phys. Res.*, A287, (1990), p. 341.
- [Jon89] Y.Jongen, C.M.Lyneis, *The Physics and Technology of Ion Sources*, Edited by I.G.Brown, ISBN 0-471-85708-4, (1989), p. 207.
- [Kit97] A.Kitagawa, M.Muramatsu, S.Yamada, T.Okada, M.Yamamoto, K.Uno, S.Biri, J.Vamosi and X.H.Zhou, *Contributed paper to ICIS97*.
- [Koi92] H.Koivisto, J.Ärje and M.Nurmia, *JYFL Annual Report*, (1992), p. 22.
- [Koi94] H.Koivisto, J.Ärje and M.Nurmia, *Nucl. Instr. and Meth. in Phys. Res.*, B94, (1994), p. 291.
- [Koi97a] H.Koivisto, J.Ärje and M.Nurmia, *Contributed paper to ICIS97*.
- [Koi97b] H.Koivisto, unpublished.
- [Knu81] H.Knudsen, H.K.Haugen and P.Hvelplund, *Phys. Rev. A*, Vol 23, Number 2, (1981), p. 597.
- [Liu92] E.Liukkonen, *13th. Intern. Conf. on Cyclotrons*, Vancouver, (1992), p. 22.
- [Lot68] W.Lotz, *Z. Phys.* 216, (1968), p. 241.
- [Lym90] W.J.Lyman, W.F.Reehl, and D.H.Rosenblatt, *Handbook of Chemical Property Estimation Methods*, American Chemical Society, Washington, DC, McGraw-Hill (1990), ISBN 0-8912-1761-0.
- [Lyn87] C.M.Lyneis, *Proc. of the 11th Int. Conf. on Cyclotrons and their Applications*, Tokyo,1987, p. 707.
- [Lyn90] C.M.Lyneis, Z.Xie, D.J.Clark, R.S.Lam and S.A.Lundgren, *Proc. 10th Workshop on ECR Ion Sources*, Oak Ridge National Laboratories, Knoxville, (1990) p. 47.
- [Mac86] M.Mack, *Proc. of the 7th Workshop on ECR Ion Sources*, Groningen, 1986, p.152.

- [Mel90] G.Melin, C.Barué, P.Briand, M.Delaunay, R.Geller, A.Girard, K.S.Golovanivsky, D.Hitz, B.Jacquot, P.Ludwig, J.M.Mathonnet, T.K.Nguyen, L.Pin, M.Pontonnier, J.C.Rocco and F.Zadworny, Proc. 10th Workshop on ECR Ion Sources, Oak Ridge National Laboratories, Knoxville, (1990), p. 1.
- [Mey85] F.W. Meyer, Nucl. Instr. Meth. in Phys. Res. B9 (1985), p. 532.
- [Mey90] F.W.Meyer et. al, Proc. 10th Workshop on ECR Ion Sources, Oak Ridge National Laboratories, Knoxville (1990) p. 367.
- [Mül77] A.Müller and E. Salzborn, Phys. Lett. 62A, (1977), p. 391.
- [Mül79] A.Müller and E. Salzborn, Phys. Lett. 70A, (1979), p. 410.
- [Nak90] T.Nakagawa, T.Kageyama, E.Ikezawa, M.Hemmi, and Y.Miyazawa, Proc. 10th Workshop on ECR Ion Sources, Oak Ridge National Laboratories, Knoxville, (1990) p. 163.
- [Nak92] T. Nakagawa, T.Kageyama, M. Kase. A.Goto and Y.Yano, Cyclotron and their Applications, Proceedings of the 13th International Conference, Vancouver, (1992), p. 365.
- [Nak93] T.Nakagawa, T.Kageyama, A.Goto, M. Kase, Y. Kanai and Y.Yano, Proc. of the 11th Int. Workshop on Electron Cyclotron Resonance Ion Sources, Groningen, May 6-7, (1993), p. 208.
- [Nak95] T.Nakagawa, T.Kageyama, M.Kase. A.Goto and Y.Yano, Jpn. J.Appl. Phys. Vol.34 (1995), p. 2463.
- [Nak96] T.Nakagawaa, J.Ärje, Y.Miyazawa, M.Hemmi, M.Kase, T.Kageyama, O. Kamigaito, T.Chiba, N.Inabe, A.Goto, and Y.Yano, contributed paper to the 5th European Particle Accelerator Conference (EPAC'96), Barcelona, June 1996.
- [Nak97] T.Nakagawa, Y.Miyazawa, M.Hemmi, M.Kase, T.Kageyama, O. Kamigaito, T.Chiba, N.Inabe, A.Goto, J.Ärje and Y.Yano, Contributed paper to ICIS97.
- [Nii95] M.Niimura, T.Kageyama, T.Nakagawa, A.Goto and Y.Yano, Proc. of the 12th Int. Workshop on ECR Ion Sources, April 25-27, RIKEN, Japan, (1995), p. 141.
- [Niim95] M.Niimura, H.Amemiya, A.Goto and Y.Yano, Proc. of the 12th Int. Workshop on ECR Ion Sources, April 25-27, RIKEN, Japan, (1995), p. 307.
- [Pos70] H.Postma, Phys. Letters, Vol. 31A, Number 4, Feb. (1970), p. 196.
- [Rot82] A.Roth, Vacuum Technology, ISBN 0-444-86027-4, (1982).
- [Shi92a] G.Shirkov, E.Donets, R.Becker and M.Kleinod, Review of the Scientific Instrumentation, 63, (1992), p. 2819.
- [Shi92b] G.Shirkov, Nucl. Instr. and Meth. in Phys. Res., A322, (1992), p. 161.

- [Shi95] G.Shirkov, Proc. of the 12th Int. Workshop on ECR Ion Sources, April 25-27, RIKEN, Japan, (1995), p. 110.
- [Taw87] H.Tawara and T.Kato, Atomic Data and Nuclear Data Tables, Vol. 36, No. 2, March (1987).
- [Ull97] A.Ullrich, P.Grübling, G.Zachornack, Contributed paper to ICIS97
- [Wal95] H.Waldmann and B.Martin, Nucl. Instr. and Meth. in Phys. Res., B98, (1995), p. 532.
- [Yam95] Y.Yamashita, Y.Isoya, Y.Kaneda. Proc. of the 12th Int. Workshop on ECR Ion Sources, 1995, p. 289.
- [Yok95] W.Yokota, Y.Saitoh, Y.Ishii, T.Nara and K.Arakawa, JAERI, Annual report 1995-96.
- [Ärj90] J.Ärje, V.Nieminen, J. Choinski and T.A.Antaya, Proc. of the 10th Int. Workshop on ECR Ion Sources, CONF-9011136, ORNL, Nov. 1-2, (1990), p. 343.
- [Ärj93] J.Ärje, H.Koivisto and M.Nurmia, Proc. of the 11th Int. Workshop on Electron Cyclotron Resonance Ion Sources, May 6-7, Groningen, (1993), p. 27.

APPENDIX

Commonly used symbols:

A	mass number
\bar{B}_0	external magnetic field [T]
\bar{E}_0	electric field [V/m]
\bar{n}	index of refraction
a_0	Bohr radius = $5.29 \cdot 10^{-11}$ m
C	conductance [m^3/s]
δ	density [kg/m^3]
e	elementary charge = $1.60 \cdot 10^{-19}$ C
ϵ_0	permittivity constant = $8.85 \cdot 10^{-12}$ Fm^{-1}
E_e	energy of electrons
f_p	plasma frequency [Hz]
η	coefficient of viscosity [$\text{kg}/(\text{m s})$]
I	ionization energy [eV]
I_0	Bohr energy = 13.6 eV
K	K-value of cyclotron
k	wave number
k	Boltzmann constant = $1.38 \cdot 10^{-23}$ JK^{-1}
μ	magnetic moment
M	molecule mass [g/mol]
m_e	mass of electron = $9.11 \cdot 10^{-31}$ kg
n_0	neutral density [$1/\text{m}^3$]
N_A	Avogadro constant = $6.02 \cdot 10^{23}$ mol^{-1}
n_c	cutoff plasma density [$1/\text{cm}^3$]
n_e	electron density [$1/\text{m}^3$]
N_K	Knudsen number
N_R	Reynolds number
P_{sat}	saturation pressure
q	charge state
Q	throughput
R	mirror ratio
S	pumping speed [m^3/s]
$\sigma_{q,q-1}$	charge exchange cross-section [m^2]

$\sigma_{q,l,q}$	ionization cross-section
T_e	temperature of electrons
τ_i	life time of ions
T_i	temperature of ions
t_{sat}	time required for saturation
v_e	velocity of electrons
v_i	velocity of ions
ω	microwave frequency [1/s]
ω_c	gyrofrequency [1/s]
ω_h	upper hybrid frequency [1/s]
ω_p	plasma frequency [1/s]
z	atomic number